

UNCLASSIFIED

AD 408 919

DEFENSE DOCUMENTATION CENTER

FOR

SCIENTIFIC AND TECHNICAL INFORMATION

CAMERON STATION, ALEXANDRIA, VIRGINIA



UNCLASSIFIED

NOTICE: When government or other drawings, specifications or other data are used for any purpose other than in connection with a definitely related government procurement operation, the U. S. Government thereby incurs no responsibility, nor any obligation whatsoever; and the fact that the Government may have formulated, furnished, or in any way supplied the said drawings, specifications, or other data is not to be regarded by implication or otherwise as in any manner licensing the holder or any other person or corporation, or conveying any rights or permission to manufacture, use or sell any patented invention that may in any way be related thereto.

DSAS-TDR-62-109

⑤ 17 505

N-63-4-2
REPORT NO.
TDR-930(2240-20)TR-1

408919

AIR FORCE ^R
TECHNICAL DATA CENTER

TECHNICAL LIBRARY

408 919

① 25
4

Document No. 62-6-432

Copy No. 1

Materials and Structures Program

High Mach Phase II

Arc Plasma Investigations and Arc Tunnel Materials Studies

SEMIANNUAL TECHNICAL REPORT

(Period Covering 1 July-31 December 1961)

28 FEBRUARY 1962

Prepared by D. J. SPENCER

Aerodynamics and Propulsion Research Laboratory

Prepared for DEPUTY COMMANDER AEROSPACE SYSTEMS

AIR FORCE SYSTEMS COMMAND

UNITED STATES AIR FORCE

Inglewood, California

AD No.
DUO FILE COPY

LABORATORIES DIVISION •

AEROSPACE CORPORATION
CONTRACT NO. AF 04(647)-930

7.60

62 6 432

④ 47.

⑤ 17 505

① DCAS TDR 62-109

① Report No. TDR 930 2240 20 TR 1

① MATERIALS AND STRUCTURES PROGRAM,
High Mach Phase II,
Arc Plasma Investigations and Arc Tunnel Materials Studies,

① NA
① NA
① 20 11
① NA
① NA
① NA
① NA

① SEMIANNUAL TECHNICAL REPORT
(Period Covering 1 July - 31 December 1961)

① 28 February 1962

Prepared by
D. J. Spencer
Aerodynamics and Propulsion Research Laboratory

AEROSPACE CORPORATION
El Segundo, California

① Contract No. AF 04(647)-930

Prepared for
DEPUTY COMMANDER AEROSPACE SYSTEMS
AIR FORCE SYSTEMS COMMAND
UNITED STATES AIR FORCE
Inglewood, California

Report No.
TDR-930(2240-20)TR-1


MATERIALS AND STRUCTURES PROGRAM
High Mach Phase II: Arc Plasma Investigations
and Arc Tunnel Materials Studies

SEMIANNUAL TECHNICAL REPORT
Period Covering 1 July - 31 December 1961

Prepared by


D. J. Spencer
Advanced Propulsion and
Fluid Mechanics Department

Approved by


J. G. Logan, Director
Aerodynamics and Propulsion,
Research Laboratory

AEROSPACE CORPORATION
El Segundo, California

FOREWORD

Section II of this report, Facilities Description and Improvements, was prepared by D. J. Spencer and K. E. Starner; Section III, Arc Power Control Systems, by K. E. Starner; Section IV, Arc Calibration and Diagnostic Techniques, by W. Welsh; and Section V, Ablation Studies, by S. Lafazan and W. Welsh. Photographs were supplied by G. H. Moore.

ABSTRACT

Progress in the Materials and Structures Program, High Mach Phase II: Arc Plasma Investigations and Arc Tunnel Materials Studies, for the period 1 July through 31 December 1961, is described. During this period, buildup of the 2-Mw arc tunnel facility was continued. Attachment of the large vacuum pumping system, cooling system, and power supply to the 200-kw tunnels was completed. This allows expansion to larger diameters (~2 in.) in the test section and longer duration test runs (~10 min). Fabrication of a Gerdien arc, intended to serve as the future plasma source in materials tests, was initiated. Arc calibration and diagnostic techniques to be employed are discussed.

The 200-kw arc tunnel facility has been utilized during this reporting period in a continuing materials testing program. Re-entry materials tested included: Graphite cloth-phenolics, ^{and} MMM Scotchply No. 202, GE 223C, and GE 523C. Discussion of the testing program for the first two materials is presented herein. The studies of GE 223C and GE 523C are classified and will be reported on in a separate document.

CONTENTS

I.	BACKGROUND INFORMATION	1
II.	FACILITIES DESCRIPTION AND IMPROVEMENTS	3
	A. Battery Power Supply	3
	B. Water Cooling System	13
	C. Vacuum System	14
	D. Gas Supply System	16
	E. Arc Tunnel Components	20
	F. Control Console	20
	G. The 200 kw Tunnel	23
III.	ARC POWER CONTROL SYSTEMS	29
	A. Constant Power System	29
	B. Trajectory Simulation Control	31
IV.	ARC CALIBRATION AND DIAGNOSTIC TECHNIQUES	39
	A. General	39
	B. Static Pressure	39
	C. Static Temperature	41
	D. Chemical Species	41
	E. Velocity	41
	F. Stagnation Pressure	42
	G. Stagnation Enthalpy	42
V.	ABLATION STUDIES	43
	A. Introduction	43
	B. Analytical Models	43
	C. Overall Energy Balance at the Char-Gas Interface	45
	D. Surface Recession Rate	46
	E. Char Layer	47

CONTENTS (Continued)

F.	Reaction Layer	48
G.	Transient Analysis	49
H.	Ablation Test Results	51
VI.	TECHNICAL PLANS, ARC TUNNEL PROGRAM	59
Table I.	Ablation Test Results	54
	NOMENCLATURE	61
	REFERENCES	64

FIGURES

1	Location of Arc Facility Subsystems	4
2	2-Mw Power Supply Main Control Panel Showing the System Electrical Schematic	5
3	2-Mw Power Supply Battery Room.	7
4	2-Mw Power Supply Switch Gear Room.	8
5	2-Mw Power Supply Bank Switching Cubicle	8
6	2-Mw Power Supply Disconnect Cubicle (Rear View).	9
7	2-Mw Power Supply Air Circuit Breakers.	9
8	2-Mw Power Supply Distribution Switch Gear, Link Panel, and Resistor Tap Switch	11
9	2-Mw Power Supply Resistor Tower	11
10	Ballast Resistor Grids	12
11	2-Mw Power Supply Station Power Control Cubicle and Overcurrent Protection Panel.	12
12	Water Cooling System Pumps on Top of the Reservoir	15
13	Water Cooling System Isolation Valves and Reservoir Tank; Vacuum Ducting and Vacuum Isolation Valve	15
14	Vacuum Pump Room and Transfer Console	17
15	Vacuum Pump System Characteristics	18
16	Gas Supply System	19
17	2-Mw Arc Tunnel Facility	21
18	2-Mw Arc Tunnel	21
19	2-Mw Arc Plasma Generator	22
20	2-Mw Tunnel Control Console	22
21	Optical Viewing System	24
22	Instrumentation Console	25
23	200-kw Arc Tunnel Facility	27
24	Gerdien Arc Parts	28
25	Gerdien Arc Assembled.	28
26	Constant Power Control.	30
27	Sliding Graphite Contactor Test Unit	32

FIGURES (Continued)

28	Contact Resistance as a Function of Current Density for Stationary Graphite Contactor	33
29	Rotating Tube Variable Resistor Test Unit	36
30	Proposed Variable Resistor for Trajectory Simulation Control	38
31	Arc Generator with Pressure Tap Nozzle Installed on Tunnel. .	40
32	Ablation Model, Zones of Interest	44
33	Ablation Test Configuration	52
34	Typical Result of Film Data Analysis	56
35	Scotchply Model after Typical Ablation Test	58

SECTION I
BACKGROUND INFORMATION

The High Mach Number and Materials Research Program was initiated in 1957 by Space Technology Laboratories, Inc., with the primary objective of developing and constructing facilities useful for the investigation of the interaction of materials with high enthalpy gas streams. The primary purpose of these studies was to advance the state-of-the-art of re-entry nose cone materials.

The basic facilities constructed in the initial stages of this program were a hypersonic shock tunnel and a 200-kw arc tunnel. A second 200-kw tunnel was later constructed. Thereafter, the program scope was broadened to include investigations of materials capable of withstanding the high-pressure high-enthalpy environments encountered in ballistic missile flow systems.

This necessitated the development of a high-pressure high-power arc operating in the 2 Mw range. Construction of this facility was completed during the period reported on here.

Thus, a fundamental program is being conducted by the Aerospace Corporation to investigate phenomena associated with the high-energy flow environments encountered by missile and space systems. The 200-kw tunnels are currently utilized in a continuing series of material tests. Primary efforts, during the remainder of Fiscal Year 1962, will be concentrated on the checkout of the 2-Mw arc facility and the initiation therein of turbulent heat transfer studies in reacting dissociating flows. Arc improvement and development investigations will be carried out with the primary objective of improving arc heater efficiency in order to raise the obtainable gas enthalpy level considerably above its present capability. Achievement of this goal will allow simulation of orbital and super-orbital lifting re-entry.

In addition, attempts will be made to program arc power for trajectory simulation in order to study the transient ablation of materials during simulated re-entry from orbital and super-orbital missions.

Diagnostic techniques will continue to be developed in order to obtain precise information about the state of the gas in the test section.

SECTION II
FACILITIES DESCRIPTION AND IMPROVEMENTS

A major effort for the current reporting period has centered around completion of the 2-Mw arc tunnel facility. The subsystems and tunnel have all been assembled and individually checked out, but the system as a whole has not been operated. A general description of the facility subsystems is given in the following subsections. See Figure 1 for the location of the subsystems.

A. Battery Power Supply

The dc power supply capable of delivering 2 Mw of power to an arc was designed and built under a contract awarded to the Nic-L-Silver Battery Co. Robert H. Wenzel of EPCO, Santa Ana, California, was the chief engineer. The power source consists of 320 batteries of 210 amp-hr rating, arrayed in 16 banks of 20 batteries each. These batteries actually constitute two power supplies, of 8 banks of 20 batteries, each capable of supplying power to the laboratories through two "hot" lines and a common return. At present, however, the protective circuit breakers are located in only two of the lines so that for certain configurations only one line of the circuit is interrupted during switching. See Figure 2 for a view of the power supply main control panel with the system schematic on it.

The open circuit voltage of each bank is 250 v. The entire array may be connected in several series and parallel arrangements to give the following open circuit terminal voltages and associated 30-sec maximum load currents:

<u>Voltage (v)</u>	<u>Current (amp)</u>
250	6400
500	6600
1000	3300
2000	2250
4000	1600

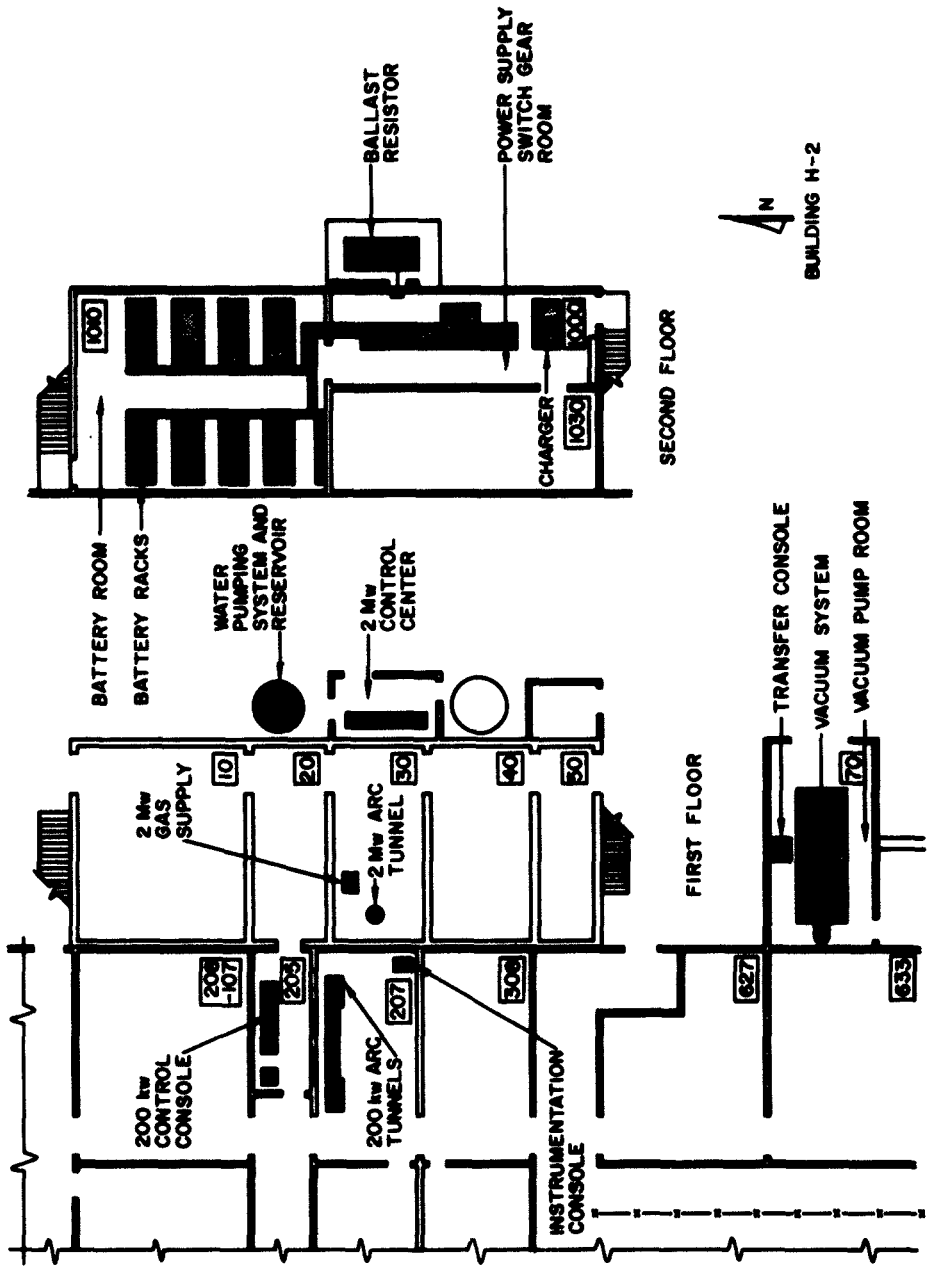


Figure 1. Location of Arc Facility Subsystems



Figure 2. 2-Mw Power Supply Main Control Panel Showing the System Electrical Schematic

In addition, voltage levels of 1500, 2500, 3000, and 3500 v are available at reduced output power. The batteries are arrayed on wooden racks impregnated with acid resistant paints. For the safety of the personnel, disconnect switches are located at the outermost end of each rack. This allows disconnection of each bank of 20 batteries into two separate banks of 10 with open circuit terminal voltage of 125 v. The 125-v terminals are then separated by the entire rack, whereas, the 250-v terminals are but a few feet apart. Battery cables utilizing 3/0 conductor rise from the racks to the cable trays suspended from the ceiling, in which they are channeled into the switch gear room (see Fig. 2 and 3). The 3/0 cables will carry 1850 amp for 30 sec with a resultant conductor temperature rise of 80°C. The cables enter the bank switching cubicle and connect to electrically controlled contactors (see Fig. 4). Here the switching of the banks in the various series and parallel arrangements occurs before connection to the main bus bars which lead to the disconnect switches. The disconnect cubicle is shown in Figure 5. From the disconnects, power is fed through the air circuit breakers, to the link panel (see Fig. 6 and 7). The ballast resistor is here connected to one of the lines via proper link arrangement. The links attach to the distribution bussing system which transverses four distribution switch gear bays. Two of the bays are not functional at this time but were included for future expansion. The other two bays contain switches which transfer power to the cables leading to the 200-kw arc tunnel in Room 207 of Building H-2 and the 2-Mw arc tunnel in Room 30 (see Fig. 1). Manipulation of the distribution switches requires the use of two keys which are held only by cognizant laboratory personnel. In addition, the switches are electrically interlocked such that the circuit breakers may be energized only at the console where control is maintained of that laboratory to receive the power. The ballast resistor consists of 20 air-cooled nichrome grids supported in a duct through which 60,000 cfm of air passes when the resistor is in operation. The three 36-in. diameter rotary blowers that pump the air have a common shaft and are powered by a 50-hp single motor. A counter-balanced lid covers the grid housing when



Figure 3. 2-Mw Power Supply Battery Room

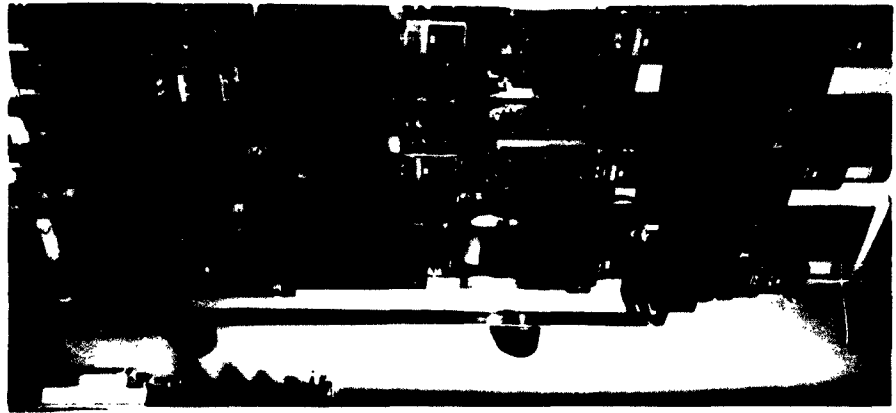


Figure 5. 2-Mw Power Supply Bank Switching Cubicle

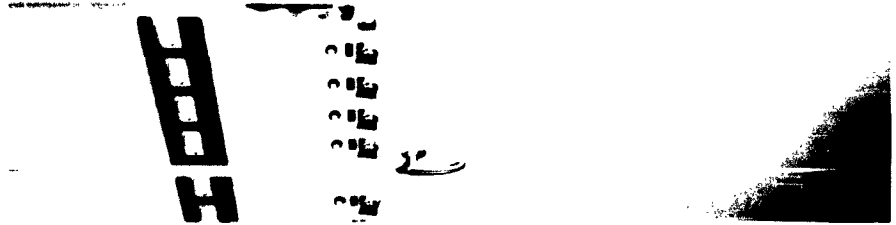


Figure 4. 2-Mw Power Supply Switch Gear Room



Figure 6. 2-Mw Power Supply Disconnect Cubicle (Rear View)

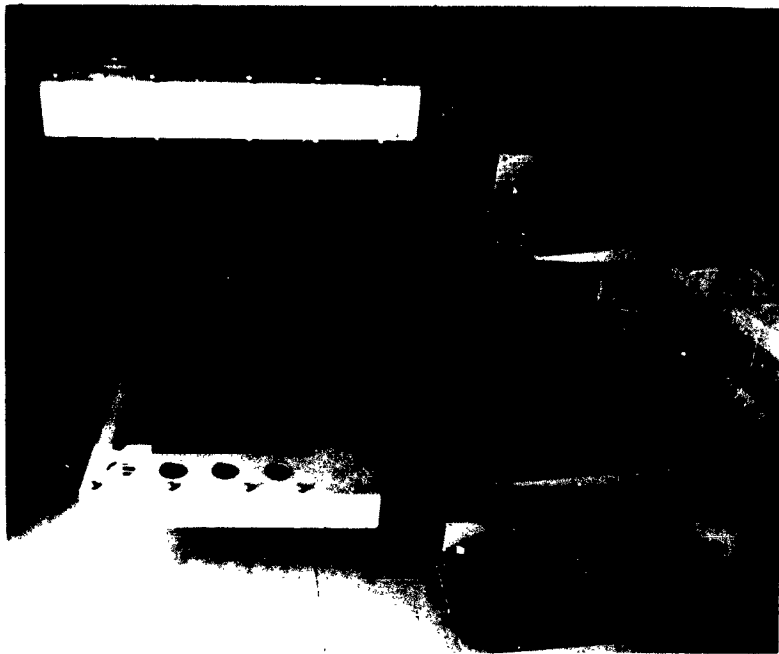


Figure 7. 2-Mw Power Supply Air Circuit Breakers

not in use and is opened at the time of blower start-up through duct overpressure. A switch closed by a vane suspended in the duct air stream is wired to the power system in order to provide a safety interlock against dissipating power in the grids without cooling. The entire assembly is mounted on a platform which also serves as the roof of the 2-mw control center.

A 10-position selector switch located inside the switch gear room adjacent to the resistor link cabinet is used in selecting the desired ballast resistance. Available resistance values range from 0.05 on Tap 1 to 0.5 on Tap 10 in 0.05 increments. As much as 1500 kw may be dissipated in the grids at each setting. The most poorly cooled portion of a resistor grid ribbon was determined by an optical pyrometer to be at 2250°F when the resistor was operating at full load. The ballast resistance change in going from no load to full load was required by original specification (and met in checkout tests) to be less than 3 percent total resistance change for the remainder of a run after the first 3 sec (see Fig. 8, 9, and 10).

Twenty batteries are used as a station power source for operation and control of the switch gear, interlock and relay circuitry, indicator light and annunciator control, et cetera. These batteries are under constant trickle charge from the plant ac power. This auxiliary battery source secures the system against industrial ac power failure during test runs.

The 320 batteries are charged in the 250 v array with 16 banks in series by the Perkins rectifier previously used in the laboratory to charge the 200-kw battery power supply. Automatic regulation of the charged current is maintained through feedback control of a saturable reactor which increases the rectifier terminal voltage as the battery banks come up to charge. All banks are released from charging at the same time. The station power control cubicle together with the overcurrent protection panel are shown in Figure 11.

Batteries installed in the facility were of special construction. The Nic-L-Silver Battery Company, to whom the entire power supply construction

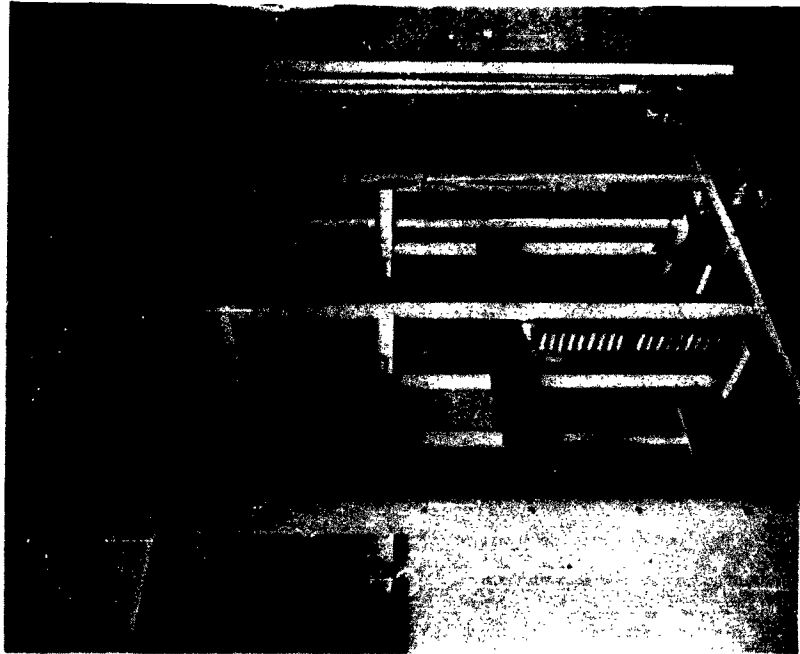


Figure 8. 2-Mw Power Supply Distribution Switch Gear, Link Panel, and Resistor Tap Switch

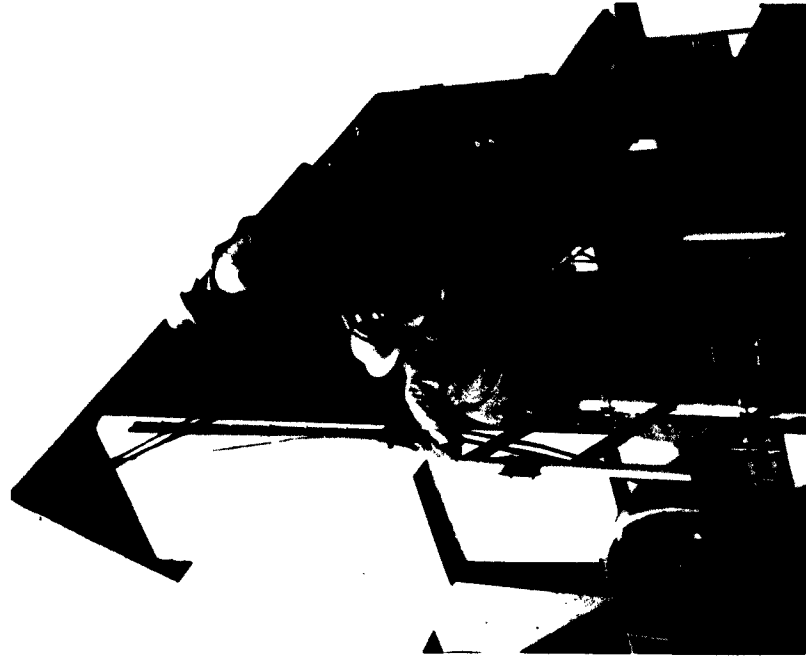


Figure 9. 2-Mw Power Supply Resistor Tower

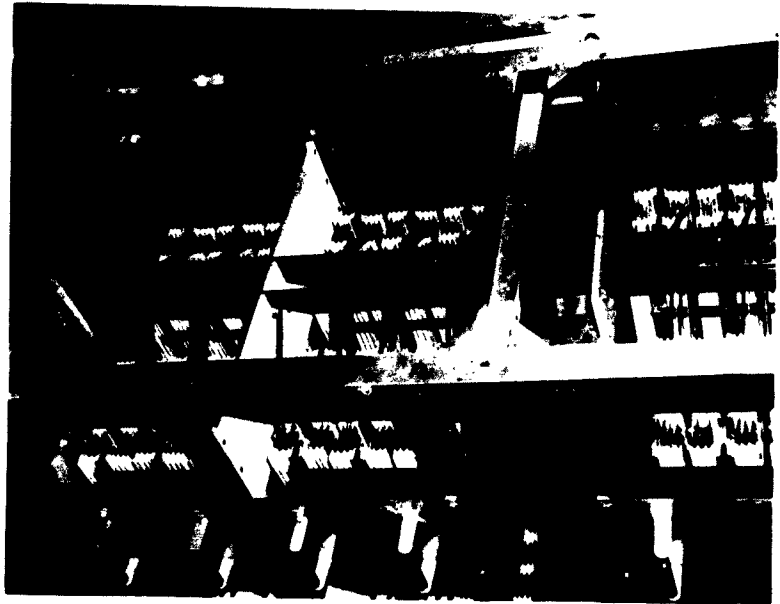


Figure 10. Ballast Resistor Grids
(courtesy R. H. Wenzel)



Figure 11. 2-Mw Power Supply Station Power
Control Cubicle and Overcurrent
Protection Panel

contract was awarded, provided 27 plates instead of the usual 25 in each cell and introduced a 2-in. long x 1/4-in. diameter copper slug into the riser and a copper bus into the straps. The net results of these changes were a decrease in the internal impedance of the cells, a decrease in the rate of change of internal impedance with time and load, and relief from a critical temperature problem in an uncooled portion of the riser. Each battery will deliver 10 kw of power under a condition of proper impedance match for maximum power transfer, for a period of 30 sec. This occurs at a current of 1500 amp per cell. Thus, the 320 batteries will deliver 3.2 Mw to an outside load with a maximum of 1.5 Mw allowable dissipation in the ballast. The power drop off with time is, of course, much less severe for lower power operation. In addition, constant power runs will be made at lower power levels and the charger will supplement the batteries as described in detail in Section III.

B. Water Cooling System

An underground reservoir with pipes and manifolds, et cetera, contains ~1200 gallons of distilled water which is circulated in a closed system through the heated arc tunnel parts during arc operation. The reservoir has an 800 gallon capacity at a 250 psi operating pressure. Three pumps mounted on top of the reservoir circulate the water through the tunnel assemblies and to an auxiliary heat exchanger (see Fig. 12). The largest pump has a capacity of 100 gpm at a pressure rise of 325 psi and is used to circulate water through the anode only. The smallest pump will develop a pressure rise of 10 psi and circulate 30 gpm up through the auxiliary heat exchanger located on the roof of Building H-2 where the heat energy of the water is transferred to the outside environment. The roof heat exchanger is designed to dissipate the accumulated heat content of the coolant water between runs spaced ~ 1 hour apart. The medium pump develops 75 psi at 300 gpm and circulates water through the arc cathode, nozzle-plenum, diffuser, heat exchanger, calorimeters, and model supports or other cooled items.

The entire system is operated at a static pressure of ~ 250 psi maintained by a small positive pressure pump. A reservoir tank supplies surplus water as needed while pressurizing the system and circulating the coolant. Elevated pressure is utilized in the system to increase the degree of liquid subcooling and consequently the minimum heat flux attainable with nucleate boiling in the cooled arc parts. Four remotely controlled safety valves are installed in the pipe leading to and from the water manifolds for the anode system and the manifolds for the other cooled-parts system (see Fig. 13). These pneumatically operated valves are closed in the event of water-line rupture at the arc to prevent excessive water losses. In addition, they may be closed in order to isolate the water pumping system from the 2-Mw arc tunnel. This allows the large cooling system to be used in facilities other than the 2 Mw arc. Water lines have been installed to and from the 300 gpm pipes to the 200 kw tunnel to provide long duration cooling of this smaller facility.

C. Vacuum System

Two Stoke's Model 412-H Microvac pumps formerly housed in Room 207, where they served as vacuum source for the 200 kw tunnel, were moved to the vacuum pump room. The two pumps were attached via 6-in. vacuum valves and associated ducts to the large main vacuum, bringing the total number of pumps constituting this system to 10. The ducting from this manifold to the 2 Mw tunnel has been completed according to the original design. The ducting has also been extended to the 200 kw facility in order to provide increased pumping capacity for the supersonic tests. A pneumatically controlled 12-in. diameter vacuum valve is located in each of these two branches of the ducting in order to provide leak-tight isolation of each facility. A 3-in. Mason-Neilan valve was attached to the ducting. The valve regulates the duct pressure to a desired level by allowing the entrance of room air into the duct through a diaphragm. It may be used for pressure matching of the test section pressure to the nozzle exit pressure in order to attain free jet flow.

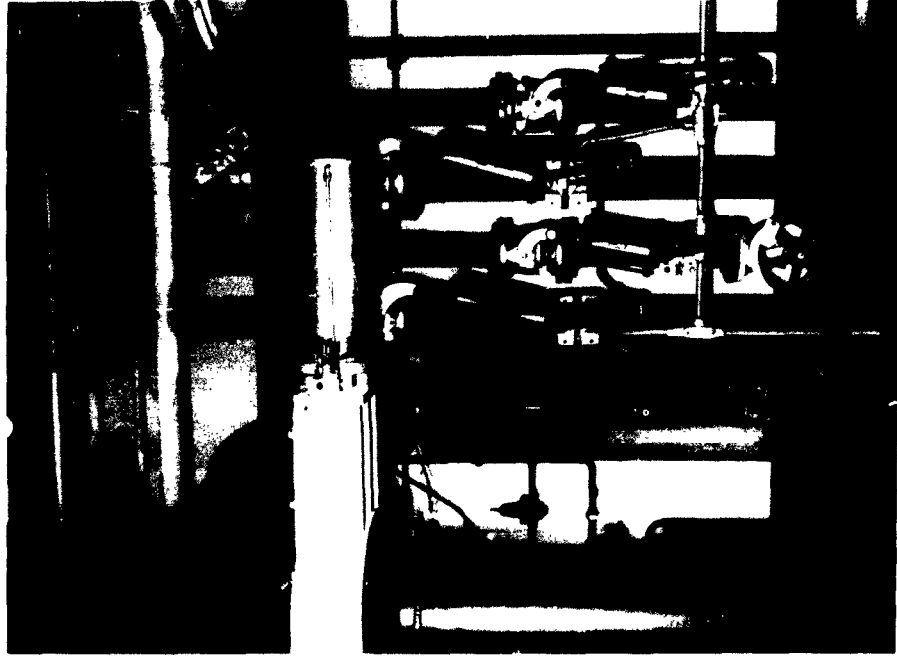


Figure 13. Water Cooling System Isolation Valves and Reservoir Tank; Vacuum Ducting and Vacuum Isolation Valve

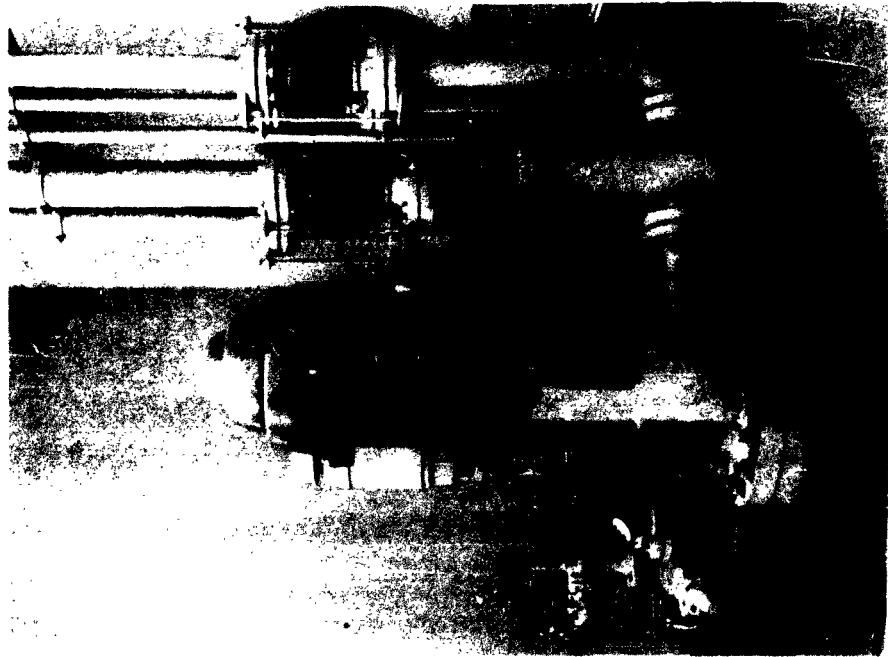


Figure 12. Water Cooling System Pumps on Top of the Reservoir

The vacuum system has one more operating "tap off" point of interest. The main manifold in the vacuum pump room has been extended through the wall into a laboratory in Building H-2 proper where it is being utilized as a pressure sink for vortex flows.

A console which transfers control of the vacuum pumps to the main control console has been completed. This transfer console is located in the vacuum pump room (see Fig. 14). It may be used either to operate the pumps manually and individually, or to start preselected pumps at 2 sec intervals in sequence at either console. In addition, this console monitors vacuum pump coolant water temperature rise and pressure drop through the pumps to insure against improper operation.

The pumping characteristics of the system were determined and are given in Figure 15.

D. Gas Supply System

The gas supply system consists of a high pressure air supply, a metering and control console, and 8 sonic injection nozzles. Flow rates of up to 100 g/sec at 300 psig metering pressure can be handled by the metering section. Three honed orifice sections are designed to meter up to 15, 40, and 100 g/sec at 10 psi maximum pressure differential. The desired orifice is selected by electrical controls on the console. Pre-run gas flow adjustments are performed at the console while control, monitoring and recording during arc runs is accomplished through electrical connections to the main control area. Figure 16 shows the gas supply system schematic. A photograph of the gas supply console is presented in Figure 17.

All pressure transducers have over-pressure protecting devices either in the form of special check-relief valves or solenoid actuating circuitry. Instrumentation is protected from regulator failure or maladjustment by use of a relief valve located in the main supply line. A pressure switch on the anode chamber assures adequate gas flow before power is supplied to the arc.

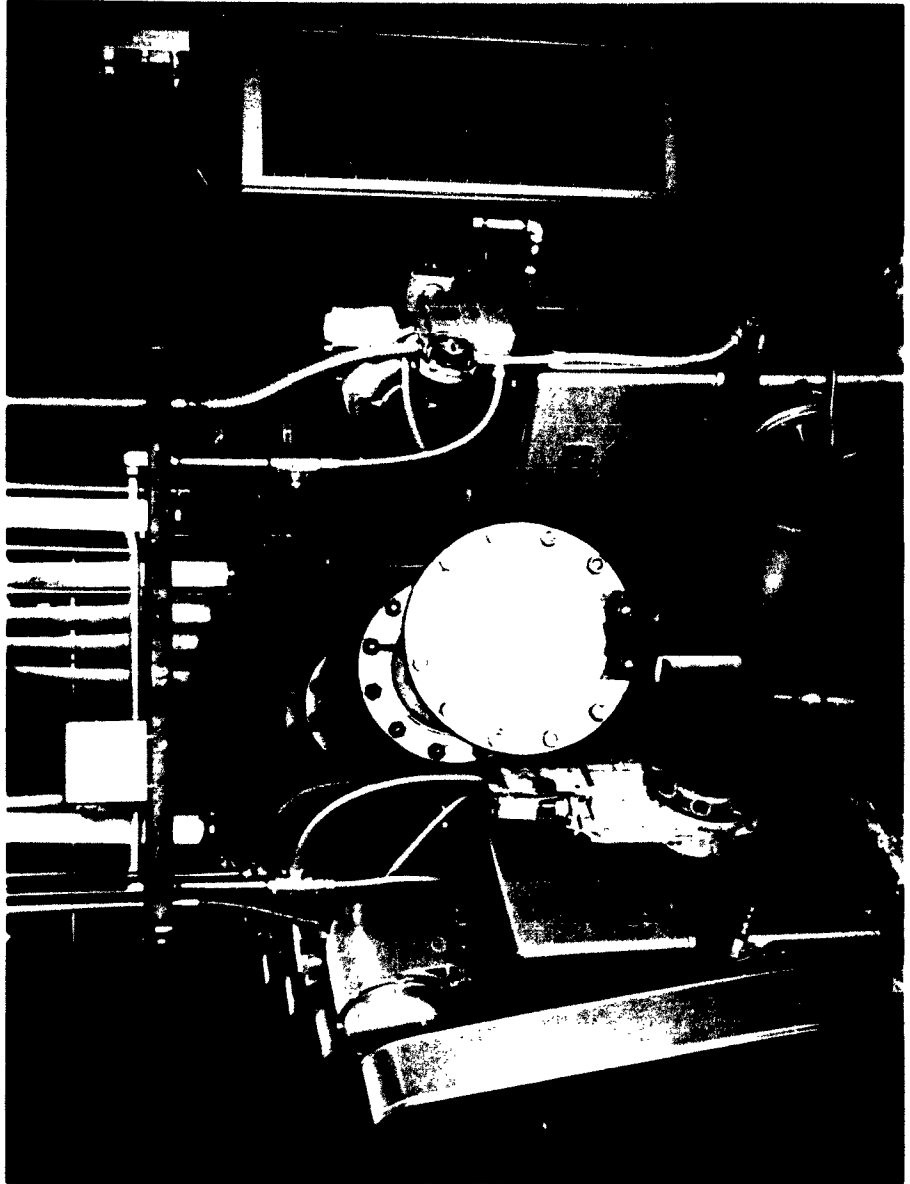


Figure 14. Vacuum Pump Room and Transfer Console

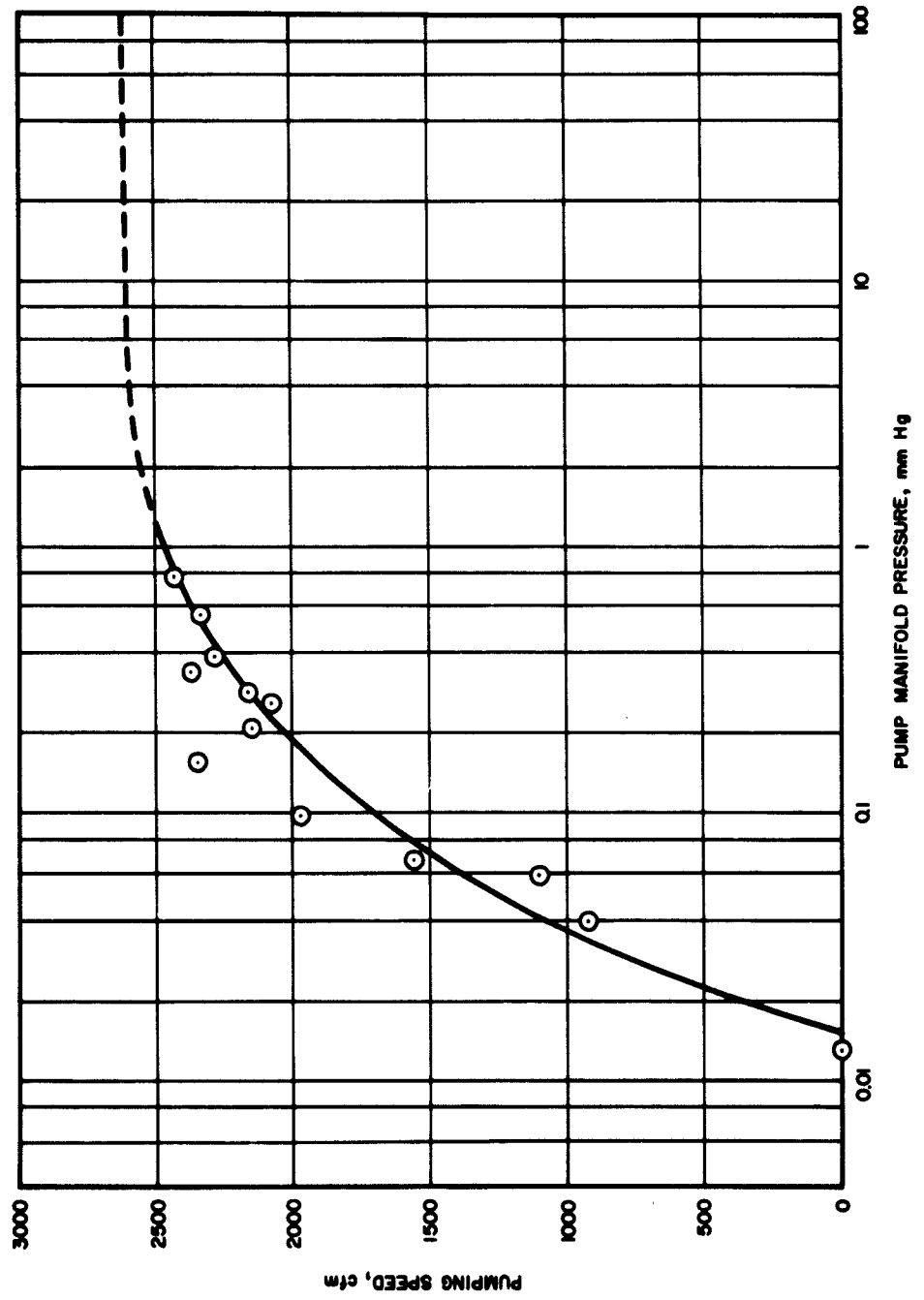


Figure 15. Vacuum Pump System Characteristics

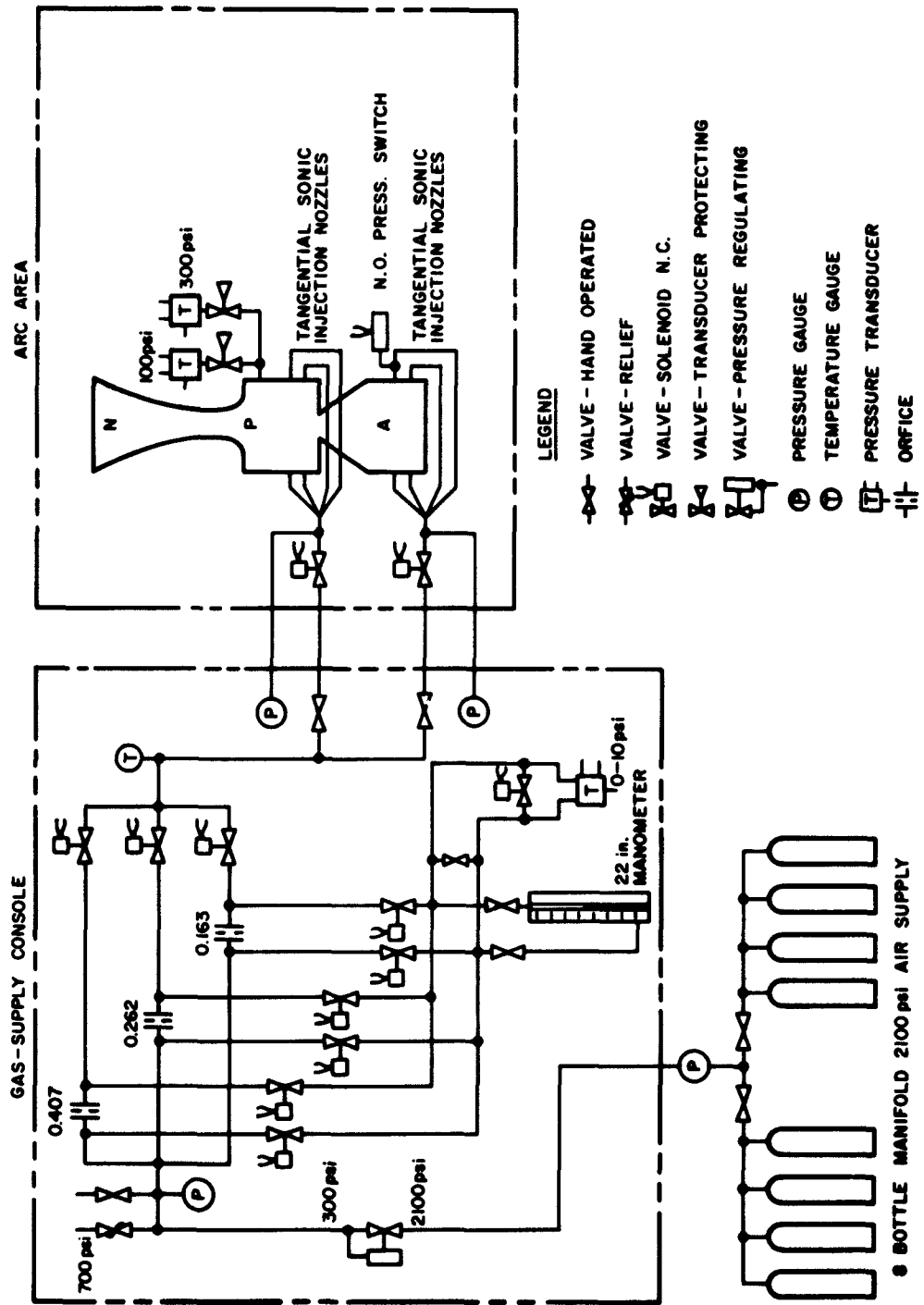


Figure 16. Gas Supply System

Four converging nozzles located in each of the anode and plenum sections provide sonic tangential gas injection for the arc unit. These nozzles have been designed to permit easy replacement for a wider range of flow rates, if necessary, without alteration of major arc components.

E. Arc Tunnel Components

Assembly and installation of the four tunnel components has been completed. The heat exchanger, consisting of a vertical array of copper tubes along which the gases flow, was designed for subsonic operation. For this reason, a diffuser was installed upstream of the heat exchanger, just downstream of the test section. The test section contains viewing windows, a port for mounting a model support, and an over-pressure relief valve. The midviewing point of the test section is ~40 in. above the floor level (see Fig. 17 and 18). Observations of a test may be made at this elevation either within the room, or from the main console, or from Room 207 through the 12-in. diameter ports in the test cell East and West walls. The plasma generator is shown in Figure 19. Water cooled coils have been added to the original basic design surrounding the arc chamber. Current flowing through the arc also flows through the coil, producing a near-axial magnetic field through the arc discharge region to work on the radial components of the arc and thereby increase the arc swirl velocity.

F. Control Console

Control of the four major subsystems, power supply, vacuum system, cooling system, and gas system is centered in the control console shown in Figure 20. The main console has control only over the closing and opening of the power supply air circuit breaker when the distribution switch gear is connected to provide power to the 2-Mw arc facility. Set up of the proper voltage and ballast resistance, and charging, et cetera, must be performed at the switch gear station. In order to provide assurance to the tunnel operator, however, the power supply terminal voltage is exhibited on a meter at the console. All four subsystems may be manually and separately controlled at the console for checkout and testing.

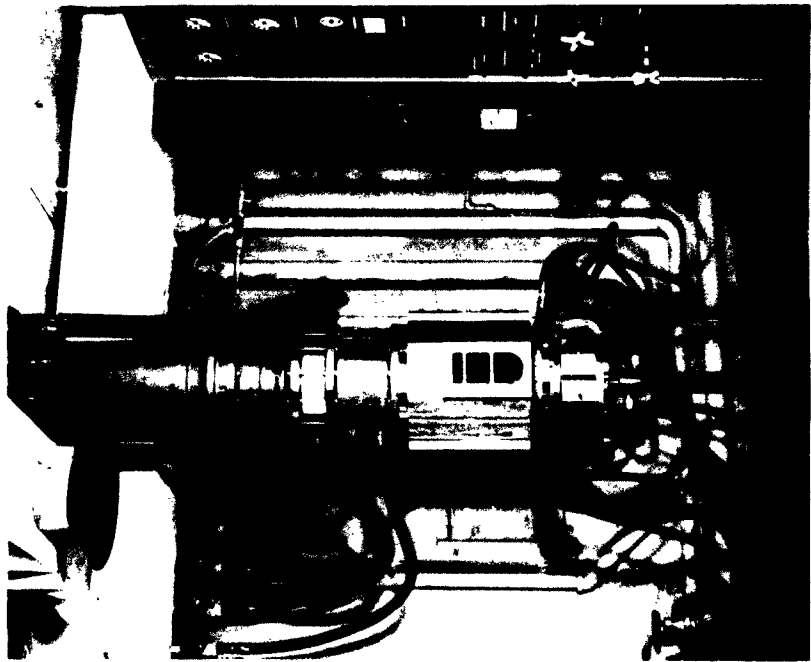


Figure 17. 2-Mw Arc Tunnel Facility

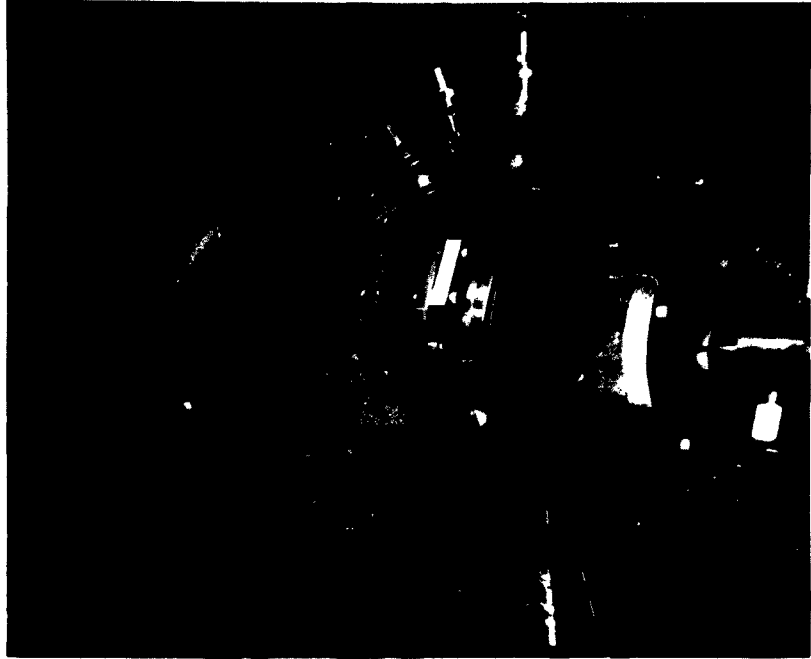


Figure 18. 2-Mw Arc Tunnel

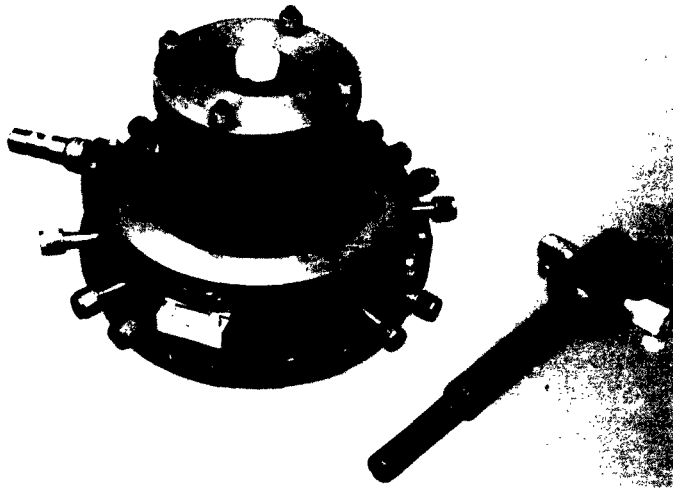


Figure 19. 2-Mw Arc Plasma Generator



Figure 20. 2-Mw Tunnel Control Console

During actual test runs, however, the control of the subsystems and the starting sequence is accomplished by the console controls. Under ideal test run conditions, the operator need only start the test with a single button press after having preselected the sequence of test operations by means of 10 timer selector switches. A view of the entire test area is available to the operator on a screen located on the console front panel. In addition, a closeup of the arc jet itself is shown in the lower left-hand corner of the screen. See Figure 21 for a schematic of the optical system. During a test the operator has a close view of the jet and a continuous Brush recording of arc current and voltage with which to detect erratic conditions during the run.

A second console, the vacuum pump power transfer console which is the center for direct control of the vacuum pumps, is located in the vacuum pump room and has been described in subsection C.

A third console resides in Room 207, outside the 2-Mw test cell, and is designated the instrumentation console. Signal leads from instrumented models, calorimeters, et cetera, are led through the cable raceways to the adjacent room and into this console for recording on the chart recorders mounted there. See Figure 22 for a view of this console.

The enthalpy computer previously designed and constructed for use with the 200 kw tunnel will also serve to compute gas enthalpy for the larger tunnel when in operation.

G. The 200 kw Tunnel

Three major changes have occurred in the 200-kw tunnel facility during this reporting period. First, with the near completion of the large 2-Mw power supply, the smaller 200-kw battery system was retired. Control for the larger power supply has been wired into the 200 kw console. This will allow longer run times. Second, the two 200-kw arc tunnels have been attached to the main vacuum supply with an attendant increase in supersonic nozzle area ratios attainable and an increase in premium laboratory space at the tunnel. Third, the large cooling system has been plumbed to the 200 kw tunnel.

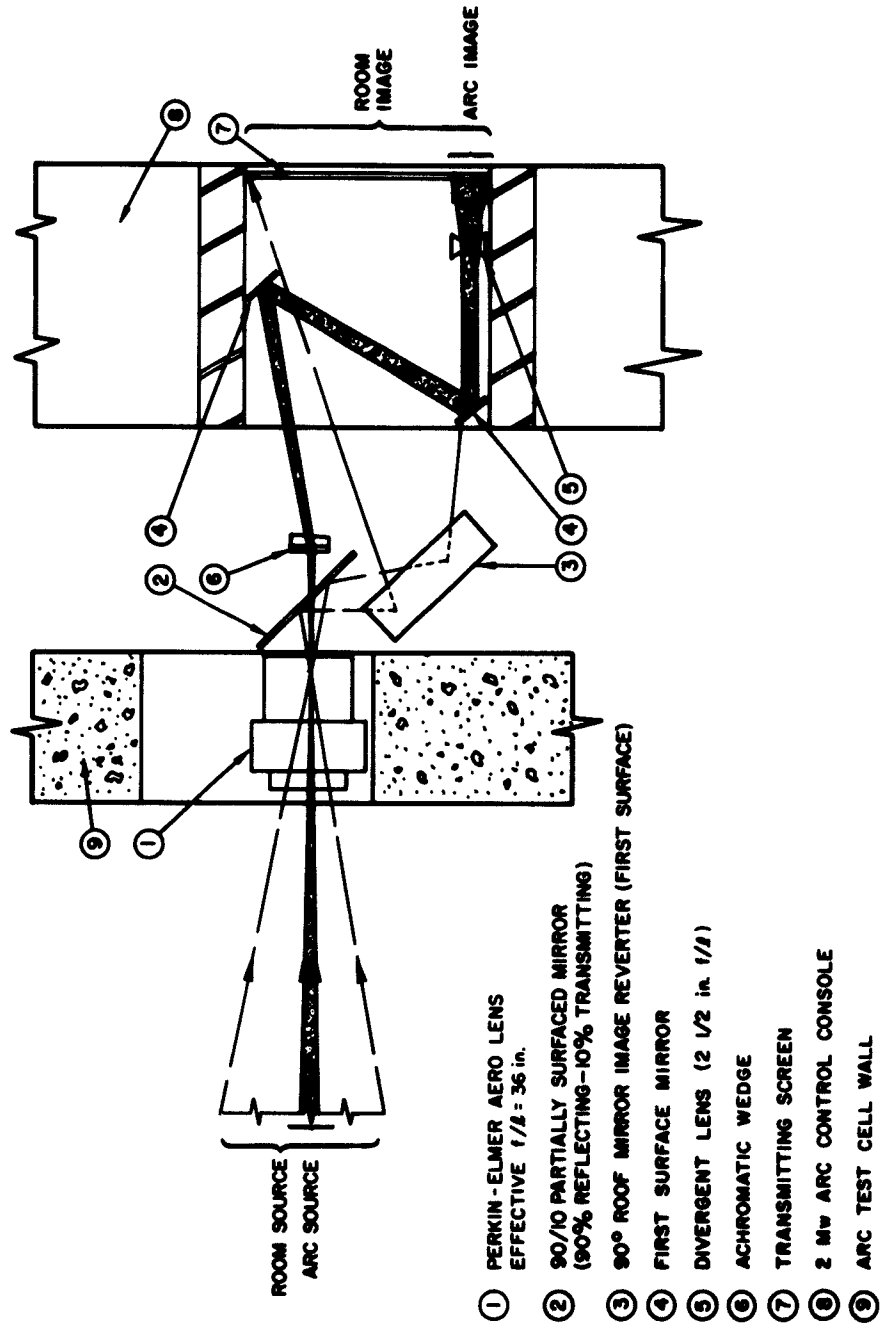


Figure 21. Optical Viewing System

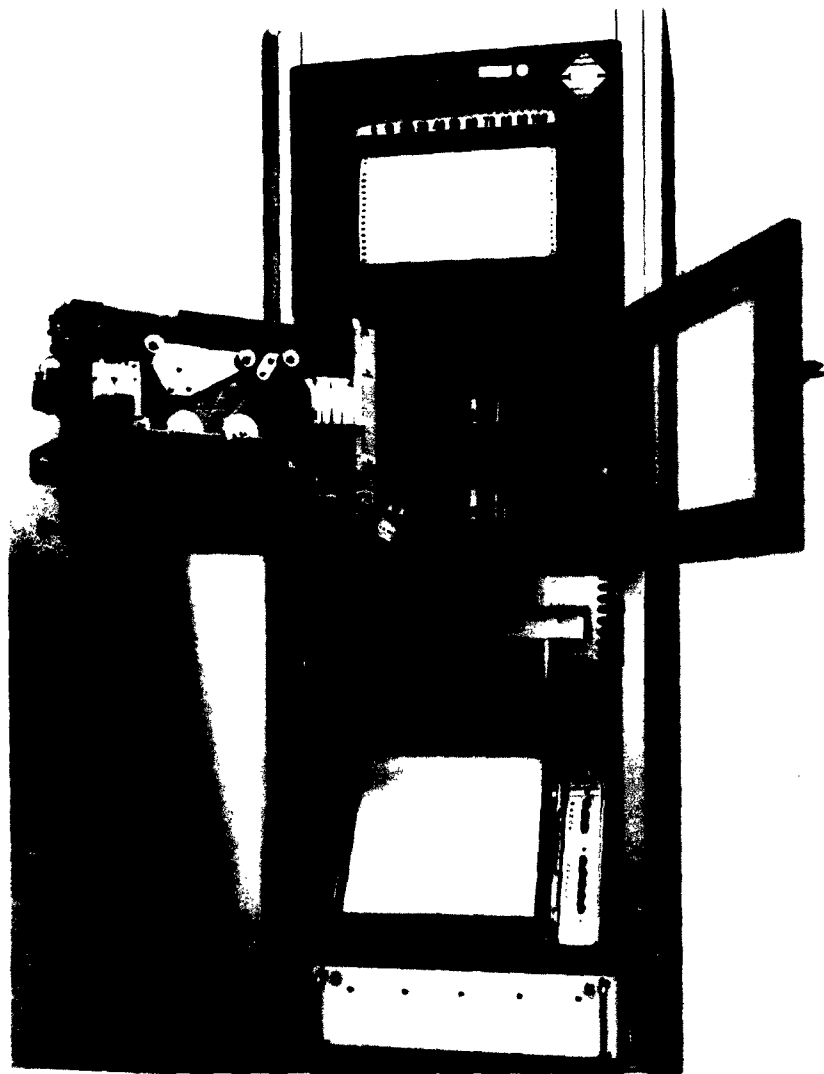


Figure 22. Instrumentation Console

This will result again in a longer run duration capability. See Figure 23 for a recent view of the 200 kw tunnel.

It is planned to incorporate a GE Gerdien-type arc in the 200 kw facility upon completion of the unit. The arc plasma generator has been fabricated and is undergoing checkout (see Fig. 24 and 25). The design received from Dr. John McGinn of GE has been adapted to our tunnel facilities, and the graphite electrodes were replaced by well cooled tungsten. In addition, the tungsten is to be sheathed with argon in a further effort to reduce electrode erosion. The Gerdien arc has as a basic design feature the attempted confinement of the electrode contamination to two plasma sheaths surrounding the electrodes emerging from the plasma generator as secondary waste jets. The useful-plasma jet exits at a point midway between the electrodes where a minimal amount of contamination is present. Values of ~ 0.01 percent have been reported.



Figure 23. 200-kw Arc Tunnel Facility

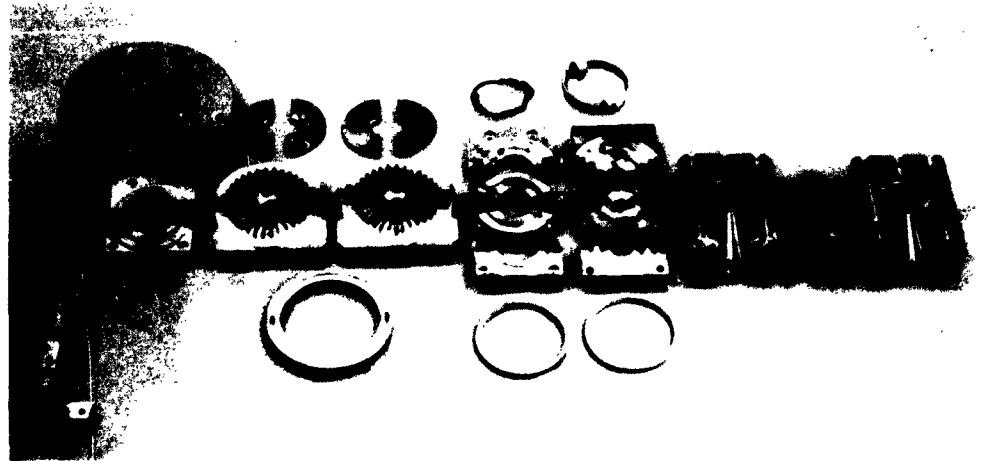


Figure 24. Gerdien Arc Parts

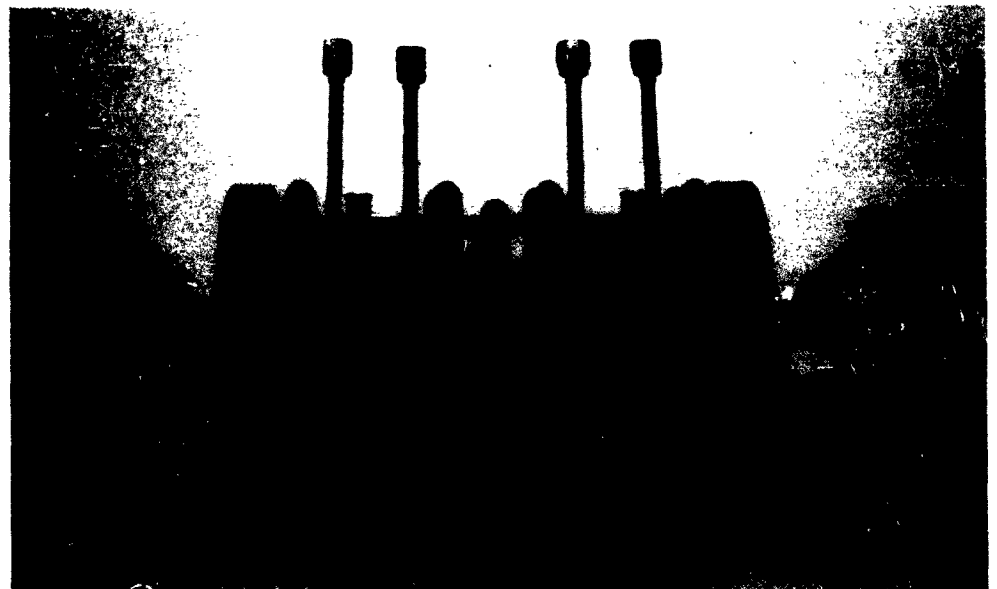


Figure 25. Gerdien Arc Assembled

SECTION III

ARC POWER CONTROL SYSTEMS

A. Constant Power System

Since the last reporting period, experimental investigations have been completed to verify the feasibility of operating the 187-kw rectifier-charger in parallel with the battery supply to obtain constant power output as battery internal impedance increases during long duration tests. It was found that, during runs of several minutes duration, the arc voltage increased as a result of cathode erosion and subsequent arc gap increase. Manual control of the cathode positioning mechanism and rectifier output produced runs of up to three and one-half minutes duration at constant arc power levels of 100 kw. Independent control of cathode and rectifier permits long duration operation at constant power with some flexibility in selection of current and voltage characteristics. The test runs were limited to a few minutes duration because of cathode burnout and lead overheating. For these tests, the arc was started and allowed to stabilize on battery operation before the rectifier was brought on the line. This method circumvents the problems encountered in attempting to start the arc with the rectified ac supply.

Figure 26 shows a schematic for a semi-automatic system permitting constant arc current and voltage control. The rectifier and meter relays become functional a few seconds after arc starting. The relay controlling arc voltage functions to advance the cathode as required to maintain constant cathode-to-anode voltage drop. Constant current is maintained by increasing rectifier output current during the run as battery current decreases as a result of internal resistance buildup. The meter relay senses any voltage decrease across the current shunt and acts to increase rectifier current. A short duration (less than one second) timer on the rectifier control prevents overshooting due to time

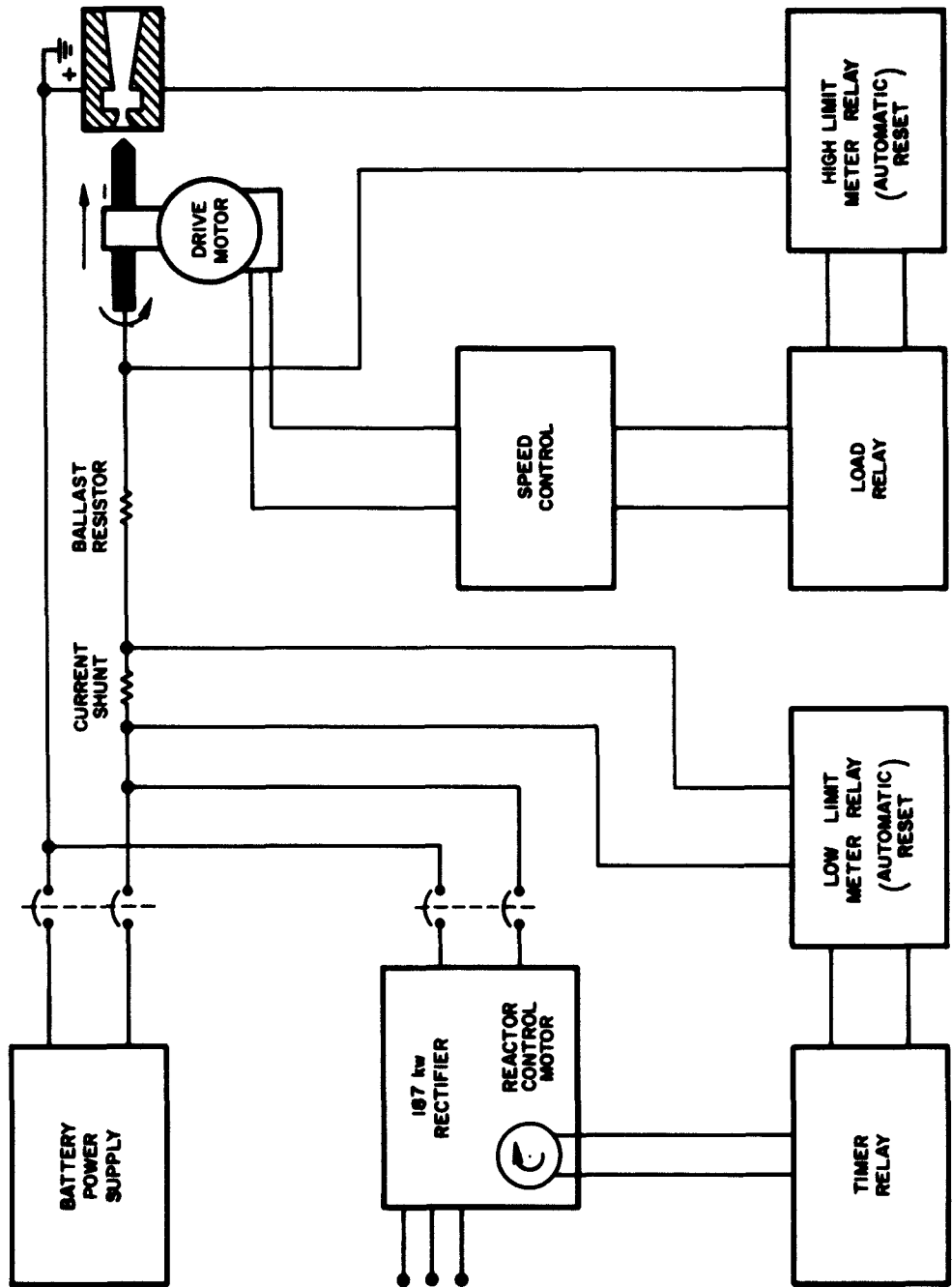


Figure 26. Constant Power Control

lag of the saturable reactor control motor. Exact control is not required to maintain constant current since extra rectifier current will simply serve to decrease battery requirements.

B. Trajectory Simulation Control

Among the problems associated with the study of transient ablation of materials during simulated re-entry is that of controlling gross power to the arc generator. One approach to this problem is to dissipate portions of the supplied power in a series resistor, thus providing either more or less arc power while operating from a fixed voltage source. To accomplish this in the present facilities it is necessary to incorporate a device capable of providing a resistance which varies continuously from essentially zero to about 0.2 ohms while carrying a current load of up to 1500 amp. This will provide a supply current variation of about a factor of 2, which reaches the upper and lower limits of stable arc operation.

A series of feasibility tests has recently been conducted to investigate several proposed methods of accomplishing this task. One method of interest is that of varying resistance by means of sliding contacts on water-cooled resistance tubing. In order to investigate the performance of this type of system, a laboratory test unit was fabricated which consisted of 2 spring loaded graphite (Type ATJ) contactors designed to slide on a horizontally mounted stainless steel tube. A photograph of this unit is presented in Figure 27. The contact surface areas were each of 0.5 sq in. Sliding of the contactors over an 8-in. travel was accomplished by manual control. Cooling water was passed through the 0.5 in. diameter tube to maintain the surface at nearly constant temperature.

Direct current of up to 200 amp was transferred through individual contactors in both stationary and sliding tests. Steady-state resistances computed from corrected voltage drops across the contactors (corrected to apply from contact area on tube to slider base) are shown in Figure 28, as functions of unit area and current density.



Figure 27. Sliding Graphite Contactor Test Unit

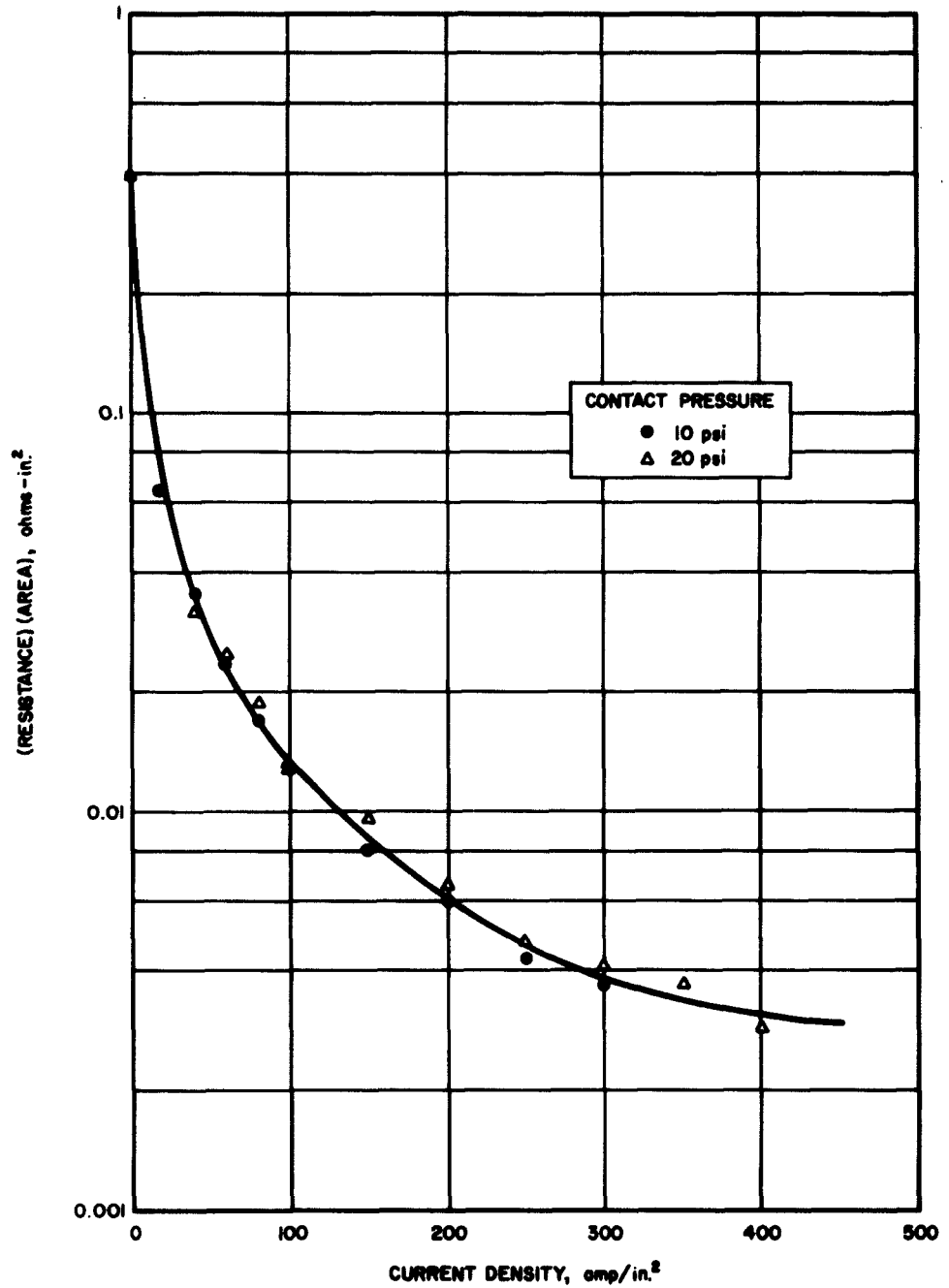


Figure 28. Contact Resistance as a Function of Current Density For Stationary Graphite Contactor

Here results are illustrated for 2 spring settings of one contactor. It is seen that contact resistance decreases over 2 orders of magnitude because of current loading and that the rate of change is greatest in the low current density range. Results for the other contact followed an identical trend, indicating that the curve is characteristic for this type of device. Heating of the contactor due to the high currents raised its temperature in excess of 500°F. As applied current was increased step-by-step, the resistance was observed to increase at first and then drop back to the values shown in Figure 28. This trend indicated a temperature effect at the junction resulting in breakdown of the contact resistance. A thermal test at zero current load verified that the decrease of contact resistance is closely associated with contactor heating.

Sliding tests of the unit were performed at speeds ranging to 10 in. per sec. It was found that sliding the contactors at zero load could change the resistance while moving by a factor of 3, whereas only about 25 percent variation was observed at high current loads. Pressure on the contact surface had considerable influence on sliding resistance at zero load but little, if any, under high currents. It is seen that current load with consequent heating of the contactor is the dominant factor, with pressure and sliding speed as secondary influences for this device.

In considering this principle for application to an arc control system, it appears that heating effects and zero load resistance variations may limit its usefulness. These effects could produce arc starting problems and also current drift during resistance changes. A different type of contactor material having a more stable contact resistance characteristic would make the device appear more attractive for this application.

Another type of device also constructed of graphite was investigated during this series of tests. This unit consisted of a stack of 5 round graphite disks (3.75 in. OD by 0.313 in. thick) of slightly concave and convex shape on alternate faces. The disks were series-connected and

stacked vertically with metal plates acting as separators. Resistance change was produced by varying an applied force on the stack by means of a gas pressure cylinder and piston arrangement. Contact pressure and area were altered with changes of the external force to produce the varying resistance. The unit was air cooled by forced convection during the tests.

With this device also, resistance was found to decrease with current density, and extensive thermal tests verified the heating effect. Correlations using the measured average disk temperature did not account for all the resistance change, therefore, it is suspected that excessive heating takes place in a thin layer adjacent to the junction surface and proceeds to break down the contact resistance. No-load resistance values were found to vary by as much as a factor of 3 as a function of positioning and separator plate deflections. Control of resistance with pressure produced a smooth variation of over a factor of 10 (0.1 to 1 ohm range) at zero load. Under current load, at average disk temperatures of 250°F and higher, the system resistance dropped more than an order of magnitude below its no-load value and exhibited no response to control pressure variations. The results of these tests would seem to eliminate this device from the control circuit of interest.

Several systems utilizing mercury contacts on water-cooled nichrome resistance tubing have been under investigation. In tests of a vertical 0.25-in. diameter tube partially immersed in a mercury bath, current densities of up to 1200 amp per sq in. were transferred at maximum currents of 450 amp. No arcing, surface oxidization, or current interruption was observed when moving the tube axially at speeds up to 2 in. per sec at the high current levels.

The success of this unit led to the development of the device shown in Figure 29. Here the mercury contact principle is utilized in a manner which lends itself well to an arc control system. Current is passed from the tube end through the tube to a small mercury well through which the

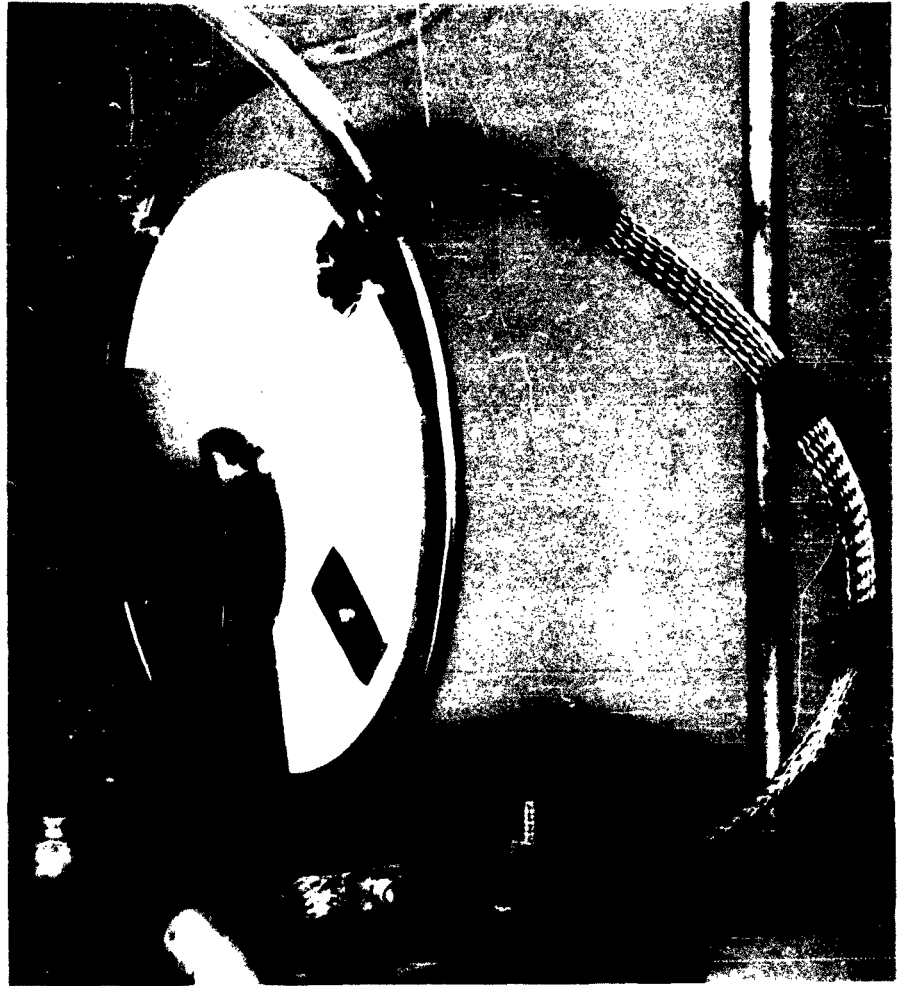


Figure 29. Rotating Tube Variable Resistor Test Unit

tube continuously passes. Change of resistance is effected by simple rotation of the tube about its mounting axis to change the active tube length. Cooling water is passed through the tube to prevent tube burn-out and mercury vaporization. This unit utilizes an 8-in. diameter tube circle and has a linear resistance of 0.0113 ohms per in.

Tests of the rotating tube device were performed mainly to determine contact resistance variations during rotation under current load. Maximum direct currents of 400 amp at tube speeds to 5 in. per sec were utilized. An X-Y recorder was used to investigate any voltage variations across the mercury contact at frequencies up to 35 cps. Results indicate that the only fluctuations present are those introduced through manual control of the instrument. Again no detrimental effects were observed either at the contact or on the tube surface. Measured resistance across the contact junction was negligible (a few milliohms) for the proposed application.

Figure 30 illustrates a possible complete unit based on the rotating tube principle, which would be applicable to an arc control system. The tubes, in a 4-parallel 4-series electrical arrangement, give the variation from zero to 0.2 ohms. Coolant channels, in a 16-parallel arrangement, give a tolerable water temperature rise at maximum power dissipation. For this system, both resistance and heat-transfer area are direct functions of tube length; thus, heat flux is constant at a fixed current level and not a function of tube position. A maximum heat flux of 2 Btu/sec-in.² is found at the 1500 amp requirement. This calls for a coolant supply of 25 gpm to give a minimum fluid velocity of 10 ft per sec. System pressure should be at least 60 psi to assure adequate subcooling at the higher power levels. A non-oxidizing atmosphere can be provided by enclosing the unit in a sealed chamber charged with dry nitrogen. Such an enclosure will also eliminate laboratory hazards inherent in the use of exposed quantities of mercury. Variation is accomplished by use of a servo motor controlled by means of a power programming system or computer enthalpy correction signal.

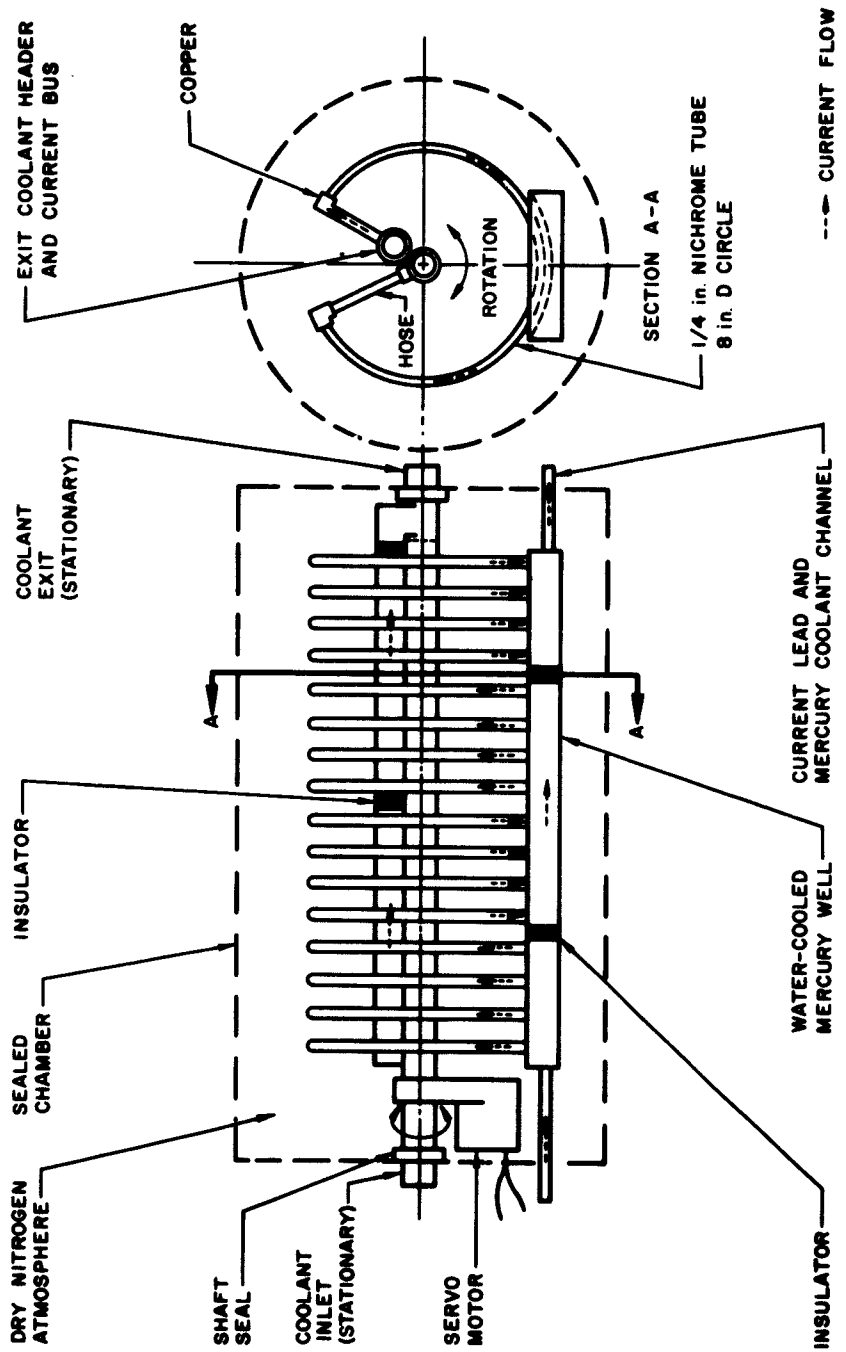


Figure 30. Proposed Variable Resistor for Trajectory Simulation Control

SECTION IV

ARC CALIBRATION AND DIAGNOSTIC TECHNIQUES

A. General

In the latter half of 1961, discussions were held to outline the need for additional arc calibrations and diagnostic methods for use with the existing 200 kw- and the nearly completed 2 mw- plasma arcs. The operational regimes of pressure and enthalpy for the available arc operating conditions will be more completely determined to facilitate establishment of testing capabilities. A number of diagnostic tools are being developed or obtained which will furnish more precise information on the state of the flow at the plasma arc exhaust. Since under certain conditions the flow in a supersonic plasma arc exhaust nozzle is not in chemical equilibrium, it is necessary to obtain an indication of the chemical state in addition to pressure and temperature measurements in order to fully describe the thermodynamic state of the flow. Spatial gradients of pressure, temperature, and chemical species exist at the plasma arc nozzle exit, primarily in the radial direction. Therefore, it is desirable to traverse the jet radius to observe the gradients in these properties. The diagnostic tools which will be used for these measurements and for kinetic and stagnation state measurements are discussed in the following subsections.

B. Static Pressure

The static pressure at the nozzle exit will be measured using small pressure taps drilled through the nozzle wall at the exit, and taps located in the downstream test section. If the supersonic jet is balanced, these pressures are equal. A nozzle with these taps has been fabricated for the 200 kw arc (see Fig. 31).



Figure 31. Arc Generator with Pressure Tap Nozzle Installed on Tunnel

C. Static Temperature

The static temperature just downstream of the nozzle exit will be measured using a spectroscopic technique described in Reference 1. This method employs a zinc tracer placed on the arc cathode whose characteristic emission lines may be used to indicate an effective temperature of the particles in the exhaust flow. The radial distribution of temperature within the jet will be derived from the spectroscopic traverse in conjunction with the Abel integral technique to account for the rotationally symmetric profile being observed.

D. Chemical Species

No method is presently available to obtain complete quantitative measurements of species present in the plasma arc exhaust. The conditions can be estimated, in part, however, in several ways. Analytical methods allow the calculation of equilibrium, completely frozen, and partially frozen expansions of the plasma flow from the stagnation condition to the exhaust condition, yielding static pressure and temperature at the exhaust for given stagnation conditions in the arc. Therefore, a simple measurement of the static pressure at the nozzle exhaust gives an indication of the chemical condition if thermal equilibrium exists between all particles. A nozzle has been fabricated with pressure taps distributed along its length to allow the comparison of pressures with the analytical results for the 200 kw arc. It is known, however, that the electrons in plasma arc flows are at a higher temperature than the other particles. To estimate the electron density and temperature, workers in this field have utilized Langmuir probes (Ref. 2 and 3) with varying degrees of success. This type of probe will also be tested in this program. Spectroscopic techniques are being studied which may allow species identification and eventually allow species concentration measurement.

E. Velocity

Brilliance fluctuations in the plasma flow have been utilized by workers in the field to measure the jet velocity. Spaced photocells and

drum camera techniques are being considered. A drum camera, available in the laboratory, needs only shutter modification.

F. Stagnation Pressure

The stagnation pressure will be measured using a simple, cooled impact tube which is on hand. A traverse mechanism has been constructed to traverse the probe tip radially across the exhaust flow.

G. Stagnation Enthalpy

A stagnation enthalpy probe developed by the Plasmadyne Corporation is being considered for use in this program. It utilizes a double cooling jacket, one part cooling a small flow drawn from the plasma exhaust to a temperature which can be measured with a thermocouple, and the other cooling the probe body. A vacuum jacket between the two water cooling flows reduces heat exchange and consequent error in the sample enthalpy calculation. A heat balance calculation yields the inlet sample enthalpy, and if the probe tip inlet area is known and constant, the product of plasma flow density and velocity can be determined from the measured plasma sample flow rate. This probe would be traversed radially across the exhaust jet to determine the radial profiles of enthalpy and mass flux. This would furnish a useful check on all other diagnostic measurements.

SECTION V

ABLATION STUDIES

A. Introduction

During this reporting period, major emphasis was placed on the analysis and testing of materials which form stable surface layers during thermal degradation. A typical class of these materials is the char-forming plastics. These materials are generally composed of thermo-setting resins (e.g., phenolic or epoxy) reinforced with either organic or inorganic fillers.

The quasi-steady and transient analysis of these materials was treated in detail and the results were reported in References 4 through 7.

The testing program was directed toward the study of basic ablation parameters needed to use and confirm the analytical ablation models. The following materials were tested: (1) Graphite cloth phenolics, (2) MMM Scotchply No. 202, (3) GE 223C, and (4) GE 523C. The studies of GE 223C and GE 523C are classified and will be reported on separately as an Aerospace Technical Report.

B. Analytical Models

The thermal degradation of a charring ablator is characterized by pyrolysis reactions in depth which yield gaseous fragments and a residual highly cross-linked carbonaceous char matrix. The fiber reinforcement is partially trapped by the char and therefore results in melting and partial vaporization of the reinforcement.

Figure 32 shows how the material may be mathematically zoned. The char matrix, char thickness, reaction zone, and the surface boundary conditions are treated briefly in the following subsections. For the detailed analysis of a charring ablator under transient and quasi-steady ablation, the reader is referred to Reference 7.

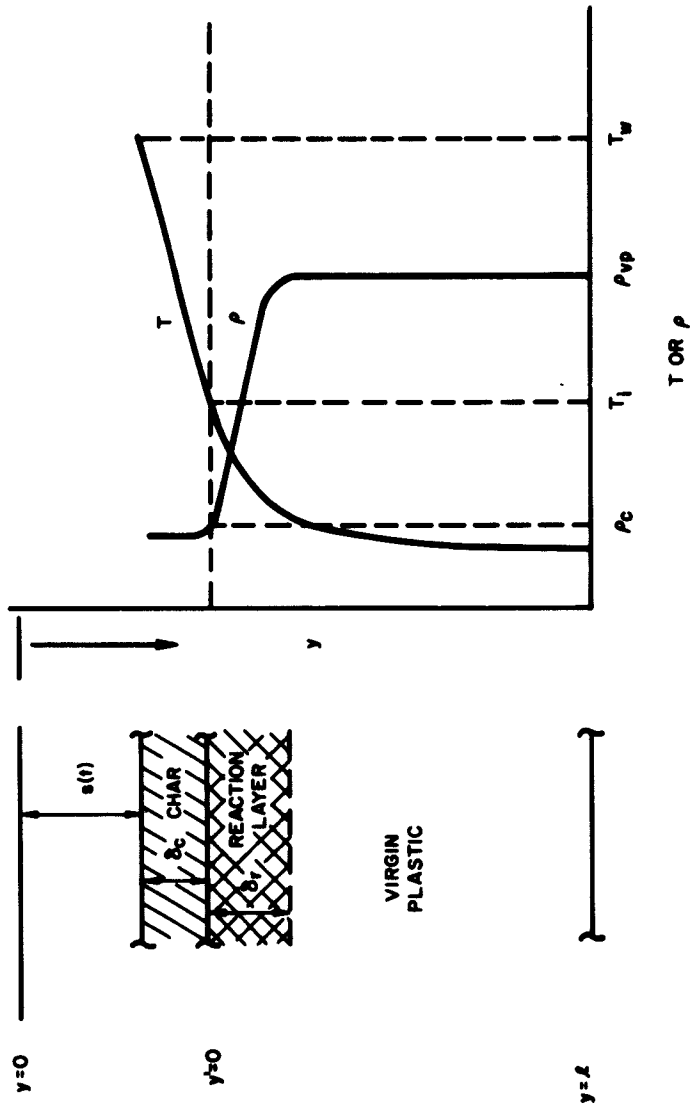


Figure 32. Ablation Model, Zones of Interest

C. Overall Energy Balance at the Char-Gas Interface

The energy balance at a gas-ablating surface interface has been treated previously in Reference 1 where it was shown that

$$(1 - \eta B)q_o + \sum_j q_{r,j} + \alpha_w q_{rad} - \sigma(\mathcal{A}) T_w^4 = \dot{m}_c \Delta H_{v,g} - k_{eff} \left(\frac{\partial T}{\partial y} \right)_y = 0, \quad (1)$$

and for quasi-steady conditions,

$$-k_{eff} \left(\frac{\partial T}{\partial y} \right)_y = 0 = \dot{m}_{vp} \Delta H_{eff} \quad (2)$$

The effective heat of ablation is then

$$Q^* = \frac{\frac{\Delta H_{eff} + f_c \Delta H_{v,g}}{\sum_l F_{l,j} C_{j,e} \Delta H_{r,j}} + \eta (H_s - H_{w,o})}{1 + \frac{j}{(H_s - H_{w,o})}} \quad (3)$$

$$= \frac{\frac{\alpha_w q_{rad} - \sigma(\mathcal{A}) T_w^4}{q_o}}{1 + \frac{\sum_l F_{l,j} C_{j,e} \Delta H_{r,j}}{1 + \frac{j}{(H_s - H_{w,o})}}}$$

The use of Equation (3) to predict the Q^* for a given material and environment requires a priori knowledge of surface chemical reactions, surface temperature, and the thermo physical properties of the material. In general, the surface temperature is not known and the overall energy balance must be used only as a boundary condition for solution of the energy equation within the ablating material.

D. Surface Recession Rate

We now consider cases where the primary mechanism for char erosion is due to chemical ablation between the char and chemically active species in the boundary layer. Under quasi-steady ablation and for conditions where (1) the char surface temperature is below the vaporization temperature of graphite ($T_s < 6600^\circ \text{F} @ 1 \text{ atm}$) and (2) the char is not lost due to mechanical failure at the char-plastic interface, the rate of chemical consumption of the char is related to the rate of ablation of the virgin plastic by

$$\dot{s}_c = \dot{s}_{vp} = \frac{1}{\rho_c} (\dot{m}_s)_w \quad (4)$$

$$\dot{s}_c = \frac{F_1}{\rho_c} \rho_e u_e C_{H_0} \beta \quad (5)$$

where

$$F_1 \triangleq \frac{(\dot{m}_s)_w}{(\dot{m}_s)_w} \quad \begin{array}{l} \text{(rate limited)} \\ \text{(diff. limited)} \end{array} \quad (6)$$

and

$$\beta = \frac{\sum_j \left(\frac{v_s \bar{m}_s}{v_j \bar{m}_j} \right) C_{j,e}}{1 + \frac{\eta}{F_c} \sum_j \left(\frac{v_s \bar{m}_s}{v_j \bar{m}_j} \right) C_{j,e}} \quad (7)$$

The effective heat of ablation is then given by

$$Q^* = f_c \frac{1}{F_1 \beta} (H_s - H_{w,o}) \quad (8)$$

It is seen from Equation (8) that, when chemical ablation is the dominant mechanism for the ablation of a charring plastic, Q^* varies linearly with $(H_s - H_{w,o})$.

E. Char Layer

Under quasi-steady ablation, the char matrix will approach a thickness, δ_c , which is related to the surface boundary conditions and the rate of depolymerization of the virgin plastic. If it is assumed that there is negligible resistance to gas flow within the char (zero pressure gradient across the char), then the char thickness may be related to the rate of ablation, the temperature difference across the char, and the thermo physical properties of the materials. The resulting solutions for the char thickness, δ_c , and the temperature distribution are

$$\delta_c = \left(\frac{f_c}{1 - f_c} \right) \left(\frac{k_{eff}}{C_{p_g}} \right) \left(\frac{1}{F_1 \rho_e u_e C_{H_o} \beta} \right) \ln \left[\frac{\Delta H_{eff}}{\Delta H_{eff} - (1 - f_c) C_{p_g} (T_w - T_i)} \right] \quad (9)$$

Functionally, Equation (9) provides a relationship between δ_c , T_w , and T_i for a given environment and material. The temperature distribution through the char is given by

$$T = T_w + \frac{\Delta H_{\text{eff}}}{(1 - f_c) C_{p_g}} \left\{ \left[\frac{\Delta H_{\text{eff}}}{\Delta H_{\text{eff}} - (1 - f_c) C_{p_g} (T_w - T_i)} \right]^{-y/\delta_c} - 1 \right\} \quad (10)$$

F. Reaction Layer

It remains to relate the rate of ablation, \dot{s} , to the temperature at the char-plastic interface. The relationship follows from consideration of a rate-limited depolymerization of the virgin plastic.

$$\dot{s}^2 = \frac{a B e^{-E_a/RT_i}}{\frac{E_a}{RT_i} \left[\left(1 - \frac{T_\infty}{T_i} \right) - \frac{\delta}{T_i} \left(1 - \frac{E_a}{RT_i} \left(1 - \frac{T_\infty}{T_i} \right) \right) \right]} \quad (11)$$

which is good for small values of δ where

$$\delta \triangleq \frac{\Delta H_{dp}}{(1 - f_c) C_p \frac{E_a}{RT_i} \left(1 - \frac{T_\infty}{T_i} \right)} \quad (12)$$

G. Transient Analysis

The preceding analysis treated the quasi-steady ablation of a charring plastic. This analysis is applicable only when the time to reach steady ablation is small in comparison to the total heat transfer period. Qualitatively, it may be shown that the time to reach steady-state ablation increases with decreasing heat transfer rate and the parameter $F_1 (T_w)$. Therefore, for certain types of ablation tests, a transient analysis must be used.

The transient ablation of a charring plastic has been treated by Munson (Ref. 6) and by Lafazan (Ref. 7); the energy equation in transformed coordinates is given by

$$\begin{aligned} \rho_p C_{p_p} \left[\left(\frac{\partial T}{\partial t} \right)_{\xi} + \frac{\dot{s}(\xi - 1)}{l - s} \left(\frac{\partial T}{\partial \xi} \right)_t \right] &= k_{\text{eff}} \left(\frac{1}{l - s(t)} \right)^2 \left(\frac{\partial^2 T}{\partial \xi^2} \right)_t \\ &+ B_1 \left(\frac{1}{l - s(t)} \right) \left(\frac{\partial T}{\partial \xi} \right)_t \left(\frac{\partial \rho_p}{\partial \xi} \right)_t \\ &+ \dot{m}_g C_{p_g} \left(\frac{1}{l - s(t)} \right) \left(\frac{\partial T}{\partial \xi} \right)_t \\ &- B \Delta H_{dp} \rho_{s_1} e^{-E_a/RT} \end{aligned} \quad (13)$$

and the conservation of mass is given by

$$\left(\frac{\partial \rho_p}{\partial t}\right)_\xi = - (1 - f_c) B \rho_{s_1} e^{-E_a/RT} + \frac{\dot{s}(1 - \xi)}{1 - s(t)} \left(\frac{\partial \rho_p}{\partial \xi}\right)_t \quad (14)$$

where

$$\xi = \frac{y - s(t)}{1 - s(t)} \quad (15)$$

and the boundary conditions are given by

$$\dot{s} = \frac{F_1}{\rho_c} \rho_e u_e C_{H_2O} \beta \quad (16)$$

$$q_o (1 - \eta_B) + \sum_j q_{r,j} + a_w q_{rad} - \sigma (A) T_w^4 = \dot{m}_c \Delta H_{v,g} - k_{eff} \left(\frac{\partial T}{\partial y}\right)_{y=s} \quad (17)$$

For detailed derivations and discussion of this analysis the reader is referred to References 6 and 7.

This set of equations has been programed for analog computation and is presently being programed for the IBM 7090 digital computer.

H. Ablation Test Results

Ablation test data were obtained using graphite cloth-phenolic resin models and models made from a proprietary material known as "Scotchply" produced by the Minnesota Mining and Manufacturing Company.

A comprehensive summary of analytical and experimental ablation test results for several ablation materials, including graphite cloth-phenolic resin material, is given in Reference 8.

The test method consisted of placing a flat-faced cylindrical model, with its axis parallel to the arc exhaust flow, in the plasma stream for a period of 30 sec to 1 min while motion pictures were taken of the model, and subsequently determining the weight loss of the model due to the ablation process. The plasma flow was subsonic air of 0.5 in. diameter compared to the 0.75 in. diameter of the model. The front face of the model was initially positioned 3 jet diameters downstream of the arc exhaust nozzle exit plane.

A schematic diagram of the test configuration is shown in Figure 33. The apparatus which held the model in position included a drive motor which translated the model holder toward the arc exhaust nozzle at a constant rate. This compensated for the recession rate of the front face of the model resulting from the ablation process, and maintained the position of the front face almost stationary with respect to the arc exhaust nozzle.

The convective heat transfer rate to a flat-faced cylinder stagnation point facing a jet of hot gas has been found to be amenable to analytical prediction for a range of distances downstream of the jet origin of approximately 3 jet diameters (Ref. 8), with the stagnation point velocity gradient being simply the ratio of jet velocity to the jet diameter. Experimentally, it is found that smaller spacings between the jet origin and the model yield higher heat transfer rates and larger spacings yield lower heat transfer rates. Therefore, it is essential that the spacing be maintained approximately constant at 3 jet diameters.

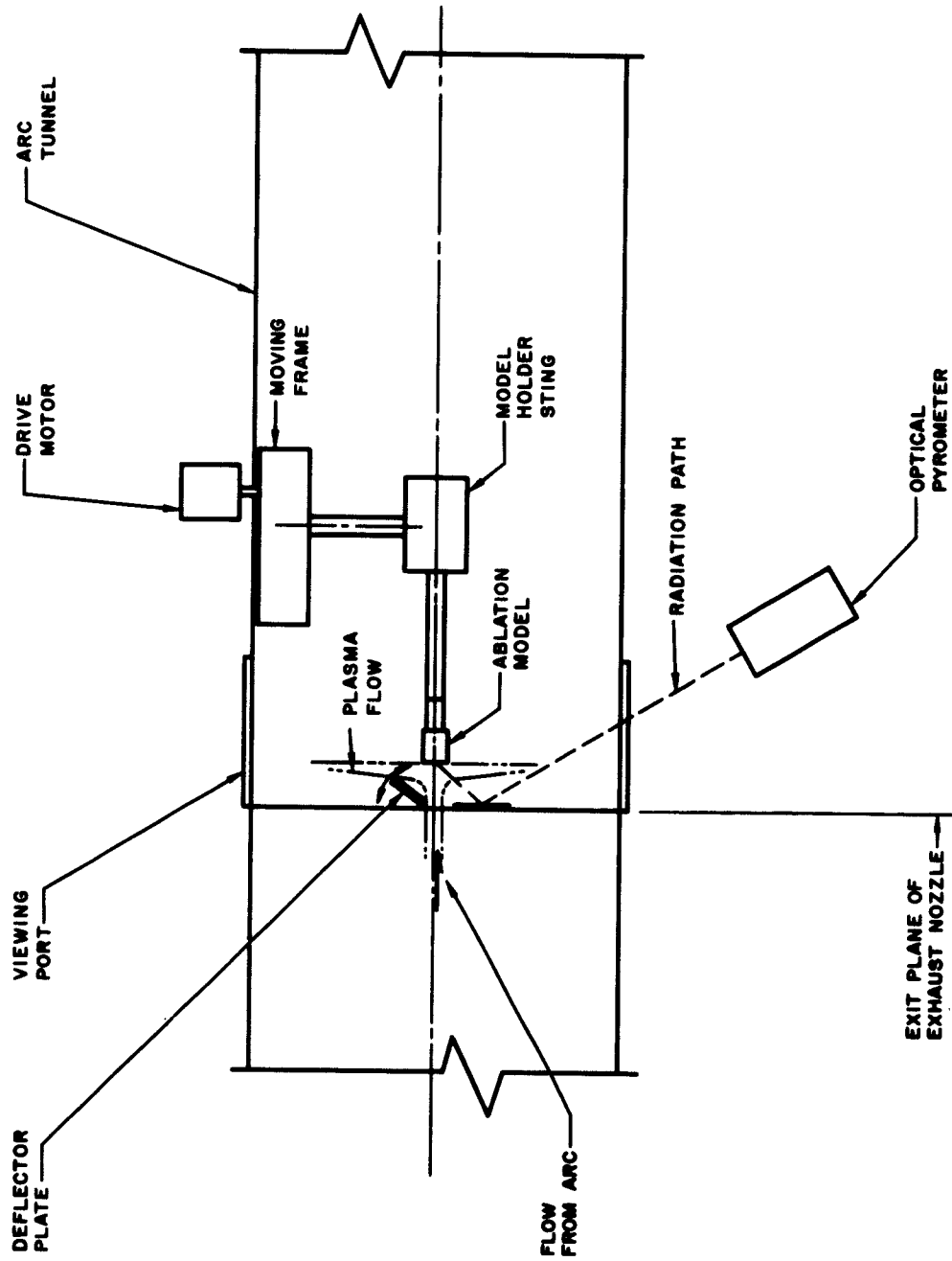


Figure 33. Ablation Test Configuration

The advantage of testing ablation models in subsonic jets is that the heat transfer rate is approximately constant across the face of a flat-faced cylinder, which allows the ablating surface to remain essentially flat during a test. In addition, the flow tends to separate from the model at the junction of the flat face with the cylindrical surface, yielding low heat transfer rates to the cylindrical side surface of the model. These conditions are such that within limits the ablation results can be compared with analytical results based on the assumption of one-dimensional phenomena.

A deflector plate, shown in Figure 33, was used to divert the plasma flow away from the ablation model until steady arc operating conditions were established. A Leeds and Northrup optical pyrometer was used to measure the apparent temperature of the ablating surface during each test. This was corrected to the actual surface temperature through a calibration method described in Reference 9.

Table I shows the results of the 3 tests using graphite cloth-phenolic resin models and the 2 tests using Scotchply models. The chemical composition of these ablation materials is shown in the table. All models used fibre orientation parallel with the model axis. The static pressure in all tests was 1 atmosphere. The gas enthalpy ranged from 3250 to 6640 Btu/lb, and the jet velocity was of the order of 1000 ft/sec in all tests. The convective heat transfer, q_o , to a solid surface at the wall temperature of the ablating surface was calculated using the relation of Fay and Riddel described in Reference 8 in order to deduce the effective heat of ablation Q_{eff}^* , defined as

$$Q^* = \frac{q_o}{\dot{m}_w} \quad (18)$$

Where \dot{m}_w is the rate of mass loss per unit area. The rate of mass loss can in turn be written as

$$\dot{m}_w = q_{vp} \dot{s} \quad (19)$$

Table I. Ablation Test Results

Results	Test No.				
	1 GCP ^a	2 GCP	3 GCP	4 3-M ^b	5 3-M
H_g / RT_o	196	96	96	92	296
$T_{\text{surface}}, ^\circ R$	5220	5392 ^c	4680	4775	5402
$q_o, \text{Btu/ft}^2 \text{sec}$	498	218	245	265	1805
Test Time, sec	40	60	30	31	22
$\dot{s}, \text{in./sec}$	0.00167	0.00222	0.00286	-- ^d	0.00639
$\rho_{vp}, \text{lb/in.}^3$	0.0505	0.0502	0.0501	0.2310	0.245
$\Delta m, \text{lb}$	0.00895	0.01367	0.00690	0.00265	0.00692
$\Delta L, \text{in.}$	--	--	0.125	--	--
$Q^*(\dot{s}), \text{Btu/lb}$	41,200	9810	11,800	--	7030
$Q^*(\Delta m), \text{Btu/lb}$	6830	2930	3270	8490	9390
$Q^*(\Delta L), \text{Btu/lb}$	--	(6800)	8100	--	--
$\dot{x}, \text{in./sec}$	0.002705	0.002940	0.003360	-- ^d	0.00727
$(H_g - H_w), \text{Btu/lb}$	4950	1557	1860	1695	4442

^a Graphite cloth-phenolic resin (27% resin by weight)
^b Scotchply material No. 202 (phenolic resin, carbon cloth, ZrO)
^c Believed to be erroneously high since $q_{\text{rad}} > q_o$ for this wall temperature
^d Negligible movement

which is true only for the case of quasi-steady ablation where the surface recession rate \dot{s} is equal to the rate of movement of the interior temperature and chemical composition fields. If no mass is lost from the sides of the model and the rate of surface recession is uniform throughout the time period of the test, then we may also write

$$\dot{m}_w = \frac{(m_i - m_f)}{(t_i - t_f)} \quad (20)$$

where m and t are mass and time respectively, and i and f are initial and final states. The Q_{eff}^* based on Eq. (19) shall be designated $Q^*(\dot{s})$ and the Q_{eff}^* based on Eq. (20) shall be designated $Q^*(\Delta m)$. The values based on both methods are indicated in Table I. Specifically, $Q^*(\dot{s})$ is obtained by determining the surface recession rate \dot{s} from analysis of the motion picture record and correcting for the motion of the model holder frame. The $Q^*(\Delta m)$ value is obtained simply from the measurements of initial and final mass and elapsed test time. A typical result of the film analysis is shown in Figure 34.

The points in Figure 34 represent the distances of the front face of the model and the front face of the "reaction zone" from the exit plane of the arc exhaust nozzle. The reaction zone is considered to be near the location where a sharp decrease in brilliance is noted just behind the front face of the model, viewing from the side. The front face of the model and the thin slab of the material just beneath the surface, representing the char zone, glowed brilliantly in these tests. Where the rates of movement of these two locations are equal, it is considered that a condition of quasi-steady ablation is established. The true rates of movement of the zones are obtained by subtracting the model holder velocity from the slopes given in Figure 34. It will be noted in Table I that the corrected rates of movement are not equal for Tests 1, 2, and 3 on the graphite cloth-phenolic resin material. They are more nearly equal in Tests 2 and 3 than in Test 1, however. The values of $Q^*(\dot{s})$ and

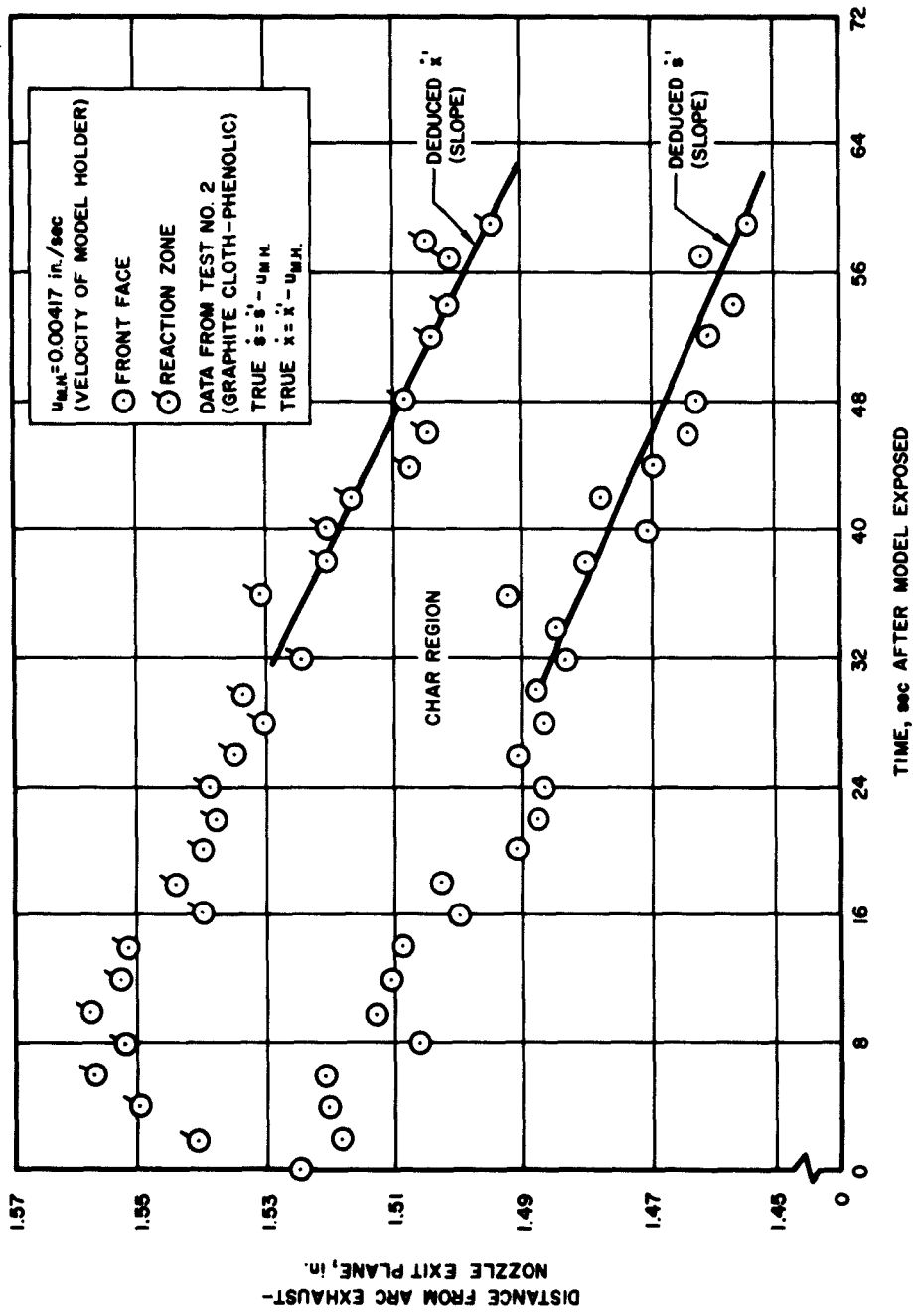


Figure 34. Typical Result of Film Data Analysis

$Q^*(\Delta m)$ are also in better agreement for Tests 2 and 3; however, the agreement is not satisfactory even for those tests.

A check was made of the integrated length change according to \dot{s} for Test 3 against a measurement of the actual length change made after the test. The integrated ΔL from the deduced \dot{s} was 0.0858 in. and the measured ΔL was 0.125 in., indicating a 45.7% greater length change than deduced from the film data corrected for model holder movement. It was also deduced from this that only 40.1% of the mass loss occurred at the front face of the model, and with that correction a value of $Q^*(\Delta L)$ was recalculated, yielding a value intermediate between $Q^*(\dot{s})$ and $Q^*(\Delta m)$.

It must be concluded that the results for effective heats of ablation of graphite cloth-phenolic resin models based on either mass loss or apparent recession rate are inconsistent. The probable cause of error for both values of Q^* is the nonquasi-steady nature of these tests, and additional possible errors are: for $Q^*(\Delta m)$, an excessive mass loss from the side surface of the model; and for $Q^*(\dot{s})$, an indeterminate thermal expansion of the model and/or model holder in the axial direction. For Test 3, however, the additional measurement of length change after the run allows the determination of a $Q^*(\Delta L)$ shown in Table I which may be considered to be reasonably accurate. Since Test 2 was made under similar conditions, an estimated value of $Q^*(\Delta L)$ was calculated for that test, assuming an identical ratio of front surface mass loss to side surface mass loss; that value is shown in parentheses in Table I as it is of questionable accuracy. Test 1 indicated front face and reaction zone movements that were quite different, and the quasi-steady Q_{eff}^* values have little significance for this test. It is also believed that the surface temperature indicated for Test 2 is erroneously high.

The Scotchply material ablated unevenly, as shown by Figure 35, a photograph of a typical sample after a test. In Test 4, the surface recession was negligible, but in Test 5 there was noticeable recession and the surface and reaction movement rates were in fair correspondence. The Q^* values are therefore reasonably accurate for Test 5.



Figure 35. Scotchply Model After Typical Ablation Test

The effective heats of ablation reported for these tests should be regarded with some caution since for no test was the quasi-steady condition clearly established. It has been shown in informal calculations, however, that often where the $Q^*(\Delta m)$ and $Q^*(s)$ values are not too different, the Q^* based on surface recession rate corresponds closely to the true Q^* obtained at much later times when the quasi-steady condition is reached. This, it is believed, results from the fact that the surface temperature usually rises close to its quasi-steady value much more quickly than does the char zone assume a constant thickness; the combustion and heat transfer rates at the surface are more strongly functions of surface temperature than of the rate of blowing of gases from the decomposing interior of the material. Forthcoming tests will show the conditions for which this correspondence may be used.

SECTION VI

TECHNICAL PLANS, ARC TUNNEL PROGRAM

Research testing on selected aspects of ablation phenomena will be continued. Tests will be made to determine the appropriate chemical reaction rate laws for combustion of char layers at low surface temperatures. Other tests will be made to compare measured temperatures in the interior of an ablating body with the results of analytical predictions for nonquasi-steady ablation, where the temperature field changes more rapidly than does the location of the ablating surface. These tests will be conducted in the 200-kw subsonic and supersonic arc tunnels, using equipment that has been developed and reported previously.

The 2-Mw arc tunnel and associated apparatus will be developed and tested for use as an operating research tool. The Gerdien arc will be installed on the tunnel and checked for proper operation. As with the existing 200-kw tunnels, an exploration will first be made of the useful operating regimes of enthalpy and pressure, preparatory to further refinement. The reliability and accuracy of the associated controls, accessories, and recording systems will be ascertained and improved if necessary.

A series of diagnostic tests will be performed on both the 200-kw and 2-Mw arc exhaust streams to determine the average and local characteristics of temperature, impact pressure, enthalpy, and chemical and electrical composition. These tests will permit more exacting definition of test conditions to be imposed by the arc stream in future research experiments.

Future research experiments will include tests on heat transfer and chemical reaction in internal and external boundary layer and separated flows provided in the arc tunnels. Attention will first be given to surface-catalyzed atom recombination at locations away from the stagnation point of bodies in supersonic flows, reattachment-point heat transfer in separated flow aft of a blunt body in supersonic flow, and surface combustion inside a

tube flow of selected reactant gases. In addition, an investigation will be made to develop a modified theory of interpretation of Langmuir probe measurements, which will be directed at improved accuracy of stagnation point tests.

The diagnostic tests referred to previously are believed to be of prime importance in this program plan. The 200-kw and 2-Mw arc tunnels are in a stage of development where research tests made without further diagnostic information would be of limited accuracy. This is the case for experiments on heat transfer, chemical reaction, ablation, and electromagnetic effects. The smaller arc tunnel has served a valuable purpose in yielding preliminary results on suitability of various ablation materials; in the future, its value and the value of the larger arc tunnel will rest largely on the extent to which diagnostic information allows accurate interpretation of test data.

NOMENCLATURE

A	area	in. ²
B	blowing parameter $\frac{\dot{m}}{\rho_e u_e C_{H_o}}$	
B_1	$\partial k_{eff} / \partial \rho_p$	Btu ft ² /lb-sec-°R
C_{H_o}	Stanton Number without mass injection	
C_p	heat capacity at constant pressure	Btu/lb-°R
E_a/R	activation energy	°R
F_1	defined by Equation (6)	
f_c	fraction of material which chars	
ΔH	enthalpy change	Btu/lb
H_s	stagnation enthalpy	Btu/lb
$H_{w,o}$	wall enthalpy	Btu/lb
k	thermal conductivity	Btu/ft-sec-°R
ΔL	length change of model	in.
l	thickness	in.
m	mass	lb
Δm	mass loss of model	lb
\dot{m}	mass rate of flow	lb/ft ² -sec
\bar{m}	molecular weight	lb/mol
Q^*	effective heat of ablation	Btu/lb
$Q^*(\Delta L)$	effective heat of ablation based on actual model length change	Btu/lb
$Q^*(\Delta m)$	effective heat of ablation based on model mass loss	Btu/lb
$Q^*(s)$	effective heat of ablation based on apparent surface recession rate	Btu/lb

NOMENCLATURE (Continued)

q	heat transfer rate	Btu/in. ² -sec
\dot{s}	rate of ablation at char surface	in./sec
\dot{s}'	apparent rate of movement of char surface as deduced from motion pictures	in./sec
$s(t)$	thickness ablated at char surface	in.
T	temperature	^o R
t	time	sec
u	velocity	ft/sec
\dot{x}	rate of movement of reaction zone	in./sec
\dot{x}'	apparent rate of movement of reaction zone as deduced from motion pictures	in./sec
y	coordinate distance	in.
α	thermal diffusivity	in. ² /sec
β	defined by Equation (7)	
δ	thickness, or defined by Equation (12)	
η	blowing coefficient	
ν	Stoichiometric coefficients	
ξ	transformed coordinate	
ρ	density	lb/ft ³
ρ_{s1}	density of unreacted plastic	lb/ft ³
σ	Stefan-Boltzmann Constant	Btu/ft ² - ^o R ⁴ -hr
$\mathcal{F}A$	radiant interchange factor	

Subscripts

c	char, or chamber
dp	depolymerization
e	outer edge of boundary layer
eff	effective
f	final

NOMENCLATURE (Continued)

Subscripts (Continued)

g	gas
i	char plastic interface, or initial
j	specie index
M. H.	model holder
o	stagnation, or chamber conditions
p	plastic (reacted and unreacted)
r	reaction
rad	radiation
s	stagnation
v	vaporization
vp	virgin plastic
w	wall
∞	infinity

REFERENCES

1. Grabowsky, W. R., and D. J. Spencer, High Temperature Arc Studies, Technical Report No. 59-0000-09934. Space Technology Laboratories, Redondo Beach, Calif., 31 December 1959.
2. Jahn, R. D., and W. F. Jaskowsky, Langmuir Probe Measurements in the Plasma Tunnel, PLR-34. Plasmadyne Corporation, Santa Ana, Calif., 7 August 1959.
3. Talbot, L., J. E. Katz, and C. L. Brundin, A Comparison Between Langmuir Probe and Microwave Electron Density Measurements in an Arc Heated Low Density Wind Tunnel, TR HE-150-186. University of California, Berkeley, Calif., 27 January 1961.
4. Scala, S. M., A Study of Hypersonic Ablation, Technical Report No. R-59-SD 438. General Electric Missile and Space Vehicle Division, Philadelphia, Penn.
5. Adams, Mac. C., "Recent Advances in Ablation," ARS Journal, 29 (9) (September 1959).
6. Munson, T. R., and R. J. Spindler, "Transient Thermal Behaviour of Decomposing Materials, Part 1 -- General Theory and Application to Convective Heating," Institute of Aerospace Sciences 30th Annual Meeting, New York, 1962.
7. Lafazan, S., and W. E. Welsh, Ablation of Charring and Non-Charring Plastics; Part 1 -- Quasi-Steady Ablation, Part 2 -- Transient Ablation, Aerospace Corporation, El Segundo, Calif. (to be published).
8. Horn, R. C., and S. Lafazan, (U) High Mach Number and Materials Research Program, Phase II, Arc Plasma Investigations and Arc Tunnel Materials Studies, Semiannual Technical Report, 1 January - 30 June 1961, TDR-594(1206-01)STR, Vol. II. Aerospace Corporation, El Segundo, Calif.
9. Spencer, D. J., S. Lafazan, R. Horn, and D. Leeds, Semiannual Report on High Mach Number and Materials Research Program, 1 January - 30 June 1960, Vol. II, STL/TR-60-V002-09205. Space Technology Laboratories, Redondo Beach, Calif.

UNCLASSIFIED

Aerospace Corporation, El Segundo, California. MATERIALS AND STRUCTURES PROGRAM, High Mach Phase II. Arc Plasma Investigations and Arc Tunnel Materials Studies. SEMI-ANNUAL TECHNICAL REPORT (Period Covering 1 July - 31 December 1961), prepared by D. J. Spencer. 28 February 1962. [64] p. incl. illus. (Report TDR-930(2240-20)TR-1; DCAS-TDR-62-109) (Contract AF 04(647)-930) Unclassified report

Progress in the Materials and Structures Program, High Mach Phase II: Arc Plasma Investigations and Arc Tunnel Materials Studies, for the period 1 July through 31 December 1961, is described. During this period, buildup of the 2-Mw arc tunnel facility was continued. Attachment of the large vacuum pumping system, cooling system, and power supply to the 200-kw tunnels was completed. This allowed expansion to larger diameters (~2 in.) in the test section and longer duration test runs (~10 min). (over)

UNCLASSIFIED

UNCLASSIFIED

Aerospace Corporation, El Segundo, California. MATERIALS AND STRUCTURES PROGRAM, High Mach Phase II. Arc Plasma Investigations and Arc Tunnel Materials Studies. SEMI-ANNUAL TECHNICAL REPORT (Period Covering 1 July - 31 December 1961), prepared by D. J. Spencer. 28 February 1962. [64] p. incl. illus. (Report TDR-930(2240-20)TR-1; DCAS-TDR-62-109) (Contract AF 04(647)-930) Unclassified report

Progress in the Materials and Structures Program, High Mach Phase II: Arc Plasma Investigations and Arc Tunnel Materials Studies, for the period 1 July through 31 December 1961, is described. During this period, buildup of the 2-Mw arc tunnel facility was continued. Attachment of the large vacuum pumping system, cooling system, and power supply to the 200-kw tunnels was completed. This allowed expansion to larger diameters (~2 in.) in the test section and longer duration test runs (~10 min). (over)

UNCLASSIFIED

UNCLASSIFIED

Aerospace Corporation, El Segundo, California. MATERIALS AND STRUCTURES PROGRAM, High Mach Phase II. Arc Plasma Investigations and Arc Tunnel Materials Studies. SEMI-ANNUAL TECHNICAL REPORT (Period Covering 1 July - 31 December 1961), prepared by D. J. Spencer. 28 February 1962. [64] p. incl. illus. (Report TDR-930(2240-20)TR-1; DCAS-TDR-62-109) (Contract AF 04(647)-930) Unclassified report

Progress in the Materials and Structures Program, High Mach Phase II: Arc Plasma Investigations and Arc Tunnel Materials Studies, for the period 1 July through 31 December 1961, is described. During this period, buildup of the 2-Mw arc tunnel facility was continued. Attachment of the large vacuum pumping system, cooling system, and power supply to the 200-kw tunnels was completed. This allowed expansion to larger diameters (~2 in.) in the test section and longer duration test runs (~10 min). (over)

UNCLASSIFIED

UNCLASSIFIED

Aerospace Corporation, El Segundo, California. MATERIALS AND STRUCTURES PROGRAM, High Mach Phase II. Arc Plasma Investigations and Arc Tunnel Materials Studies. SEMI-ANNUAL TECHNICAL REPORT (Period Covering 1 July - 31 December 1961), prepared by D. J. Spencer. 28 February 1962. [64] p. incl. illus. (Report TDR-930(2240-20)TR-1; DCAS-TDR-62-109) (Contract AF 04(647)-930) Unclassified report

Progress in the Materials and Structures Program, High Mach Phase II: Arc Plasma Investigations and Arc Tunnel Materials Studies, for the period 1 July through 31 December 1961, is described. During this period, buildup of the 2-Mw arc tunnel facility was continued. Attachment of the large vacuum pumping system, cooling system, and power supply to the 200-kw tunnels was completed. This allowed expansion to larger diameters (~2 in.) in the test section and longer duration test runs (~10 min). (over)

UNCLASSIFIED

<p>Fabrication of a Gerdien arc, intended to serve as the future plasma source in materials tests, was initiated. Arc calibration and diagnostic techniques to be employed are discussed.</p> <p>The 200-kw arc tunnel facility has been utilized during this reporting period in a continuing materials testing program. Re-entry materials tested included: Graphite cloth-phenolics, MMM Scotchply No. 202, GE 223C, and GE 523C. Discussion of the testing program for the first two materials is presented herein. The studies of GE 223C and GE 523C are classified and will be reported on in a separate document.</p>	<p>UNCLASSIFIED</p>
<p>Fabrication of a Gerdien arc, intended to serve as the future plasma source in materials tests, was initiated. Arc calibration and diagnostic techniques to be employed are discussed.</p> <p>The 200-kw arc tunnel facility has been utilized during this reporting period in a continuing materials testing program. Re-entry materials tested included: Graphite cloth-phenolics, MMM Scotchply No. 202, GE 223C, and GE 523C. Discussion of the testing program for the first two materials is presented herein. The studies of GE 223C and GE 523C are classified and will be reported on in a separate document.</p>	<p>UNCLASSIFIED</p>

<p>Fabrication of a Gerdien arc, intended to serve as the future plasma source in materials tests, was initiated. Arc calibration and diagnostic techniques to be employed are discussed.</p> <p>The 200-kw arc tunnel facility has been utilized during this reporting period in a continuing materials testing program. Re-entry materials tested included: Graphite cloth-phenolics, MMM Scotchply No. 202, GE 223C, and GE 523C. Discussion of the testing program for the first two materials is presented herein. The studies of GE 223C and GE 523C are classified and will be reported on in a separate document.</p>	<p>UNCLASSIFIED</p>
<p>Fabrication of a Gerdien arc, intended to serve as the future plasma source in materials tests, was initiated. Arc calibration and diagnostic techniques to be employed are discussed.</p> <p>The 200-kw arc tunnel facility has been utilized during this reporting period in a continuing materials testing program. Re-entry materials tested included: Graphite cloth-phenolics, MMM Scotchply No. 202, GE 223C, and GE 523C. Discussion of the testing program for the first two materials is presented herein. The studies of GE 223C and GE 523C are classified and will be reported on in a separate document.</p>	<p>UNCLASSIFIED</p>

UNCLASSIFIED

Aerospace Corporation, El Segundo, California. SUMMARY REPORT OF SYSTEM AND COMPONENT STUDIES CONCERNING THE PROPOSED CHARIOT VEHICLE (UNCLASSIFIED TITLE). Prepared by Engineering Division. 23 May 1962. [494] p. incl. illus. (Report TDR-930(2515-30)TR-1; DCAS-TDR-62-127) (Contract AF 04(647)-933) Confidential report

System design and optimization studies conducted at Aerospace Corporation in the conception, guidance, system engineering, and technical direction of the Chariot Program are summarized. The space booster system, including the two stages of the Titan II and the high-energy upper stage, is called the Chariot Space Booster System. The Titan II vehicle is 10 ft in diameter and is 90.5 ft long; it utilizes nitrogen tetroxide and an equal blend of hydrazine and UDMH as propellants. As (over)

UNCLASSIFIED

UNCLASSIFIED

Aerospace Corporation, El Segundo, California. SUMMARY REPORT OF SYSTEM AND COMPONENT STUDIES CONCERNING THE PROPOSED CHARIOT VEHICLE (UNCLASSIFIED TITLE). Prepared by Engineering Division. 28 May 1962. [494] p. incl. illus. (Report TDR-930(2515-30)TR-1; DCAS-TDR-62-127) (Contract AF 04(647)-930) Confidential report

System design and optimization studies conducted at Aerospace Corporation in the conception, guidance, system engineering, and technical direction of the Chariot Program are summarized. The space booster system, including the two stages of the Titan II and the high-energy upper stage, is called the Chariot Space Booster System. The Titan II vehicle is 10 ft in diameter and is 90.5 ft long; it utilizes nitrogen tetroxide and an equal blend of hydrazine and UDMH as propellants. As (over)

UNCLASSIFIED

UNCLASSIFIED

Aerospace Corporation, El Segundo, California. SUMMARY REPORT OF SYSTEM AND COMPONENT STUDIES CONCERNING THE PROPOSED CHARIOT VEHICLE (UNCLASSIFIED TITLE). Prepared by Engineering Division. 28 May 1962. [494] p. incl. illus. (Report TDR-930(2515-30)TR-1; DCAS-TDR-62-127) (Contract AF 04(647)-930) Confidential report

System design and optimization studies conducted at Aerospace Corporation in the conception, guidance, system engineering, and technical direction of the Chariot Program are summarized. The space booster system, including the two stages of the Titan II and the high-energy upper stage, is called the Chariot Space Booster System. The Titan II vehicle is 10 ft in diameter and is 90.5 ft long; it utilizes nitrogen tetroxide and an equal blend of hydrazine and UDMH as propellants. As (over)

UNCLASSIFIED

UNCLASSIFIED

Aerospace Corporation, El Segundo, California. SUMMARY REPORT OF SYSTEM AND COMPONENT STUDIES CONCERNING THE PROPOSED CHARIOT VEHICLE (UNCLASSIFIED TITLE). Prepared by Engineering Division. 28 May 1962. [494] p. incl. illus. (Report TDR-930(2515-30)TR-1; DCAS-TDR-62-127) (Contract AF 04(647)-930) Confidential report

System design and optimization studies conducted at Aerospace Corporation in the conception, guidance, system engineering, and technical direction of the Chariot Program are summarized. The space booster system, including the two stages of the Titan II and the high-energy upper stage, is called the Chariot Space Booster System. The Titan II vehicle is 10 ft in diameter and is 90.5 ft long; it utilizes nitrogen tetroxide and an equal blend of hydrazine and UDMH as propellants. As (over)

UNCLASSIFIED

UNCLASSIFIED	<p>defined in this study, the first-stage engine is a pump-fed system with an uprated sea-level thrust rating of 500,000 lb. The second-stage pump-fed engine produces a standard altitude thrust of 100,000 lb, and the Titan II liftoff weight is approximately 321,000 lb. The Chariot stage is approximately 9.5 ft in diameter by 18 ft in length, and utilizes fluorine and a hydrazine blend as propellants. The pump-fed engine provides 35,000 lb of thrust (vacuum) and a nominal vacuum specific impulse of 390 sec. The design weight of the Chariot stage is 34,000 lb. System studies which have been made utilizing uprated Titan II boosters show maximum payloads of 13,900 lb and 2800 lb for the 100-n-mi orbit and the 19,600-n-mi orbit, respectively. Throughout the Chariot system, particular emphasis has been placed on maximum obtainable performance and mission versatility commensurate with minimum costs, a mid-1963 launch, and a high factor of reliability.</p>	UNCLASSIFIED
--------------	--	--------------

UNCLASSIFIED	<p>defined in this study, the first-stage engine is a pump-fed system with an uprated sea-level thrust rating of 500,000 lb. The second-stage pump-fed engine produces a standard altitude thrust of 100,000 lb, and the Titan II liftoff weight is approximately 321,000 lb. The Chariot stage is approximately 9.5 ft in diameter by 18 ft in length, and utilizes fluorine and a hydrazine blend as propellants. The pump-fed engine provides 35,000 lb of thrust (vacuum) and a nominal vacuum specific impulse of 390 sec. The design weight of the Chariot stage is 34,000 lb. System studies which have been made utilizing uprated Titan II boosters show maximum payloads of 13,900 lb and 2800 lb for the 100-n-mi orbit and the 19,600-n-mi orbit, respectively. Throughout the Chariot system, particular emphasis has been placed on maximum obtainable performance and mission versatility commensurate with minimum costs, a mid-1963 launch, and a high factor of reliability.</p>	UNCLASSIFIED
--------------	--	--------------

UNCLASSIFIED	<p>defined in this study, the first-stage engine is a pump-fed system with an uprated sea-level thrust rating of 500,000 lb. The second-stage pump-fed engine produces a standard altitude thrust of 100,000 lb, and the Titan II liftoff weight is approximately 321,000 lb. The Chariot stage is approximately 9.5 ft in diameter by 18 ft in length, and utilizes fluorine and a hydrazine blend as propellants. The pump-fed engine provides 35,000 lb of thrust (vacuum) and a nominal vacuum specific impulse of 390 sec. The design weight of the Chariot stage is 34,000 lb. System studies which have been made utilizing uprated Titan II boosters show maximum payloads of 13,900 lb and 2800 lb for the 100-n-mi orbit and the 19,600-n-mi orbit, respectively. Throughout the Chariot system, particular emphasis has been placed on maximum obtainable performance and mission versatility commensurate with minimum costs, a mid-1963 launch, and a high factor of reliability.</p>	UNCLASSIFIED
--------------	--	--------------

UNCLASSIFIED	<p>defined in this study, the first-stage engine is a pump-fed system with an uprated sea-level thrust rating of 500,000 lb. The second-stage pump-fed engine produces a standard altitude thrust of 100,000 lb, and the Titan II liftoff weight is approximately 321,000 lb. The Chariot stage is approximately 9.5 ft in diameter by 18 ft in length, and utilizes fluorine and a hydrazine blend as propellants. The pump-fed engine provides 35,000 lb of thrust (vacuum) and a nominal vacuum specific impulse of 390 sec. The design weight of the Chariot stage is 34,000 lb. System studies which have been made utilizing uprated Titan II boosters show maximum payloads of 13,900 lb and 2800 lb for the 100-n-mi orbit and the 19,600-n-mi orbit, respectively. Throughout the Chariot system, particular emphasis has been placed on maximum obtainable performance and mission versatility commensurate with minimum costs, a mid-1963 launch, and a high factor of reliability.</p>	UNCLASSIFIED
--------------	--	--------------